From Department of Biosciences and Nutrition
Karolinska Institutet, Stockholm, Sweden

Peptide Nucleic Acid Conjugates as Artificial Ribonucleases: Cu^{2+} and Zn^{2+}-Dependent PNAzymes

Olivia Luige

Karolinska Institutet

Stockholm 2022

Published by Karolinska Institutet.
Printed by Universitetsservice US-AB, 2022

ISBN 978-91-8016-498-6
Cover illustration: Courtesy of Johanna Luige, the cover of this thesis depicts an artist's rendition of RNA cleavage by an artificial enzyme (PNAzyme) with its pH-rate profile in the background

Peptide Nucleic Acid Conjugates as Artificial Ribonucleases: Cu^{2+} and Zn^{2+}-Dependent PNAzymes

THESIS FOR DOCTORAL DEGREE (Ph.D.)

By

Olivia Luige

The thesis will be defended in public in the lecture hall Gene, Neo, Karolinska Institutet Flemingsberg on the 18th of March 2022 at 9 am.

Principal Supervisor:
Professor Roger Strömberg
Karolinska Institutet
Department of Biosciences and Nutrition
Unit of Organic and Bioorganic Chemistry

Co-supervisors:
Merita Murtola, PhD
Karolinska Institutet
Department of Biosciences and Nutrition
Unit of Organic and Bioorganic Chemistry

Dmytro Honcharenko, PhD
Karolinska Institutet
Department of Biosciences and Nutrition
Unit of Organic and Bioorganic Chemistry

Opponent:
Associate Professor Tuomas Lönnberg
University of Turku
Department of Chemistry

Examination Board:
Professor Ülo Langel
Stockholm University and University of Tartu
Department of Biochemistry and Biophysics (SU)
Institute of Technology (UT)

Professor Leif Kirsebom
Uppsala University
Department of Cell and Molecular Biology

Professor Jan Kihlberg
Uppsala University
Department of Chemistry – BMC

POPULAR SCIENCE SUMMARY OF THE THESIS

Our DNA represents the genetic information that informs important molecular decisions that are taken in our bodies. The information stored in DNA is passed on by producing RNA that functions as a middleman, which is then used to direct how to produce proteins that do the heavy lifting involved in biological processes. Our health and well-being rely on these molecules to function as expected so that the right messages from our genes are translated into the intended biological outcomes. However, the underlying genetic information can sometimes undergo changes and stop working as it should. Such genetic mutations can lead to devastating diseases such as Huntington's and Alzheimer's diseases, cancer, and many others.

Medicinal drugs are traditionally small molecules that interact with specific binding pockets in proteins. These small pockets in large protein targets fit with the drug molecules like a lock and key. While such small molecule drugs are the backbone of the pharmaceutical industry, they can do little to interfere if erroneous information is being passed from our genes to our proteins. When faulty genetic messages are used to make proteins, large parts of the molecular make-up of these proteins can contain mistakes, or sometimes the proteins simply cannot be produced anymore. These changes can stop the proteins from performing their intended biological role or even give them new roles with harmful consequences. Missing or faulty proteins can cause enormous damage to our health, while being a huge challenge to traditional drug discovery. But there is hope from so-called "new modalities" in the drug discovery arena. Short DNA and RNA mimics can be used to silence parts of genetic information to prevent the critical mistakes from being translated into protein compositions. These drugs are called therapeutic oligonucleotides.

Therapeutic oligonucleotides are making progress in the treatment of life-threatening diseases, both in clinical trials but also already as approved drugs on the market. Oligonucleotide drugs mimic natural DNA and RNA molecules and bind to the precise sequences of genetic information relevant to a disease. They then affect how or if biological machinery can read and pass on that information. Therapeutic oligonucleotide drugs can even destroy harmful RNA molecules by recruiting enzymes in the body that specialise in RNA degradation. When the oligonucleotide therapeutic binds to the desired RNA sequence, enzymatic degradation of precisely that RNA target can be triggered, which ensures that the faulty message in the RNA will not be passed on. Alternatively, this goal could be accomplished with more sophisticated oligonucleotide drugs that can act as artificial enzymes and therefore single-handedly destroy their RNA targets without the assistance of natural enzymes.

Development of such artificial enzymes was the central aim of this thesis. Synthetic peptide nucleic acid (PNA) molecules that mimic DNA were transformed into artificial enzymes (PNAzymes) by linking them with so-called "molecular scissors" that have the ability to cut RNA target molecules.

The most critical aspects of artificial enzymes are the speed at which they cut their RNA targets, their ability to specifically recognise the desired targets without acting on other RNA

sequences, and their compatibility with biological environments. Several types of oligonucleotide-based artificial RNA-cutting enzymes have been developed in the past, but they typically suffer from slow activity and/or reliance on metal cofactors that are not naturally present in biological environments.

In the first part of this thesis, previously developed PNAzymes that require the presence of copper ions were investigated further. The RNA and PNAzyme sequences were modified, and their chemical composition varied in critical ways, revealing some interesting insights into the RNA cleavage activity of copper PNAzymes. These artificial enzymes are exceptionally efficient, but free copper is not present in biological environments and thus these PNAzymes should be mainly considered as potential tools for molecular biology research.

Zinc is a desirable metal cofactor due to its presence in biological environments, but artificial enzymes that rely on zinc ions have typically been much slower at cutting their RNA target sequences. In this thesis, efficient zinc PNAzymes were developed by embedding novel "molecular scissors" into the PNAzyme structure. These zinc-dependent artificial enzymes were shown to outperform even the best copper-dependent PNAzymes. These PNAzymes can cut half of their RNA targets in only 10 minutes, and they are highly specific – they make just one cut at a specific location in each RNA target. Their sequence has an important role in enabling their fast activity, but they can also be designed to target different RNA sequences of medical importance.

Artificial enzymes could be used to treat not only genetic disorders, but also infectious diseases by destroying the viral or parasitic RNA sequences, while leaving the human RNA untouched. Our zinc PNAzymes were shown to efficiently degrade RNA models from the malaria parasite and from the SARS-CoV-2 virus. Targeting the messenger RNA molecules in the malaria parasite can seriously impact the parasite's ability to survive, because the production of necessary proteins can be stopped. On the other hand, SARS-CoV-2 is an RNA virus and thus uses RNA as its primary genetic material which can be directly destroyed. One important aspect of the PNAzyme action is the requirement for sufficient levels of zinc in the surrounding environment. Coincidentally, zinc ions are also needed for the life cycle of the malaria parasite. Thus, zinc has been shown to accumulate to extreme levels in malaria-infected red blood cells, making malaria a particularly interesting candidate for future PNAzyme therapeutics. The efficient degradation of these clinically relevant RNA models by the zinc PNAzymes is encouraging and future work should focus on testing these PNAzymes in a biological setting to determine their efficacy in potentially treating infections and other serious illnesses.

EESTIKEELNE POPULAARTEADUSLIK KOKKUVÕTE

DNA molekulid esindavad meie geneetilist informatsiooni, millel põhinevad bioloogised protsessid meie kehas. Geenides peituv informatsioon antakse kõigepealt üle RNA molekulidele, mis omakorda annavad selle üle valkudele. Just nende biomolekulide ehitusblokkide järjestus on see, mis määrab, kuidas valgud kui tõelised töömesilased oma ülesannetega hakkama saavad. Selle informatsioonijada täpne ülekanne geenidest kuni valkudeni on meie tervise vundament, mis tagab, et õige geneetiline sõnum tõlgitakse ette nähtud bioloogiliseks tulemuseks. Kahjuks võib geneetilises informatsioonis mõnikord esineda mutatsioone – keemilisi muudatusi, mille tõttu jääb õige sõnum nende biomolekulide informatsiooniahelas edastamata või edastatakse hoopistükis vigane sõnum. Geneetilised mutatsioonid võivad viia raskete haiguste tekkeni nagu näiteks Huntingtoni ja Alzheimeri tõved, vähid ja paljud muud haigused.

Traditsioonilised ravimid on väiksed molekulid, mille märklauad on seondumistaskud valkudes. Need ravimid seonduvad oma valkudes paiknevate märklaudadega, sobitudes sinna nagu võti lukuauku. Sellised traditisioonilised ravimid on ravimitööstuse selgroog, kuid paraku pole nende tavapärastel töömehhanismidel võimalik takistada vigase informatsiooni edasi kandumist geenidest valkudesse. Valgud, mis on toodetud vigase geneetilise materjali põhjal, võivad kaotada võime täita neile ette nähtud rolli või nende koostis võib olla muutunud niivõrd, et neil on uued kahjulikud omadused. Suutmatus õigeid valke toota või nende asemel vigaste valkude tootmine viivad raskete tervisehäireteni, millele on keeruline ravi leida. Siiski on uusi lootust andvaid kandidaate ravimiarenduses, eriti just lühikeste DNA-d ja RNA-d matkivate molekulide näol. Selliseid ravimeid nimetatakse terapeutilisteks oligonukleotiidideks ning neid saab kasutada geneetilise informatsiooni vaigistamiseks viisil, mis võimaldab muuta valkude tootmiseks antavaid valesignaale.

Terapeutilised oligonukleotiidid on täiskäigul alustamas oma edulugu haiguste ravis – mitmed oligonukleotiitidel põhinevad ravimid on saanud heakskiidu ning paljusid uuritakse kliinistest uuringutes. Oligonukleotiidid on sünteetilised molekulid, mis matkivad looduslikke DNA ja RNA molekule, mistõttu saab neid suunata seonduma täpselt nende geneetilise informatsiooni järjestustega, mis on seotud haiguste tekkega. Nad saavad mõjutada kuidas või kas bioloogilised nanomasinad saavad lugeda ja edastada DNA-s ja RNA-s leiduvaid geneetilisi sõnumeid. Terapeutilised oligonukleotiidid suudavad isegi kaasa tuua kahjuliku RNA hävitamise, värvates kehas leiduvaid RNA lagundamisele spetsialiseerunud ensüüme, mis omakorda tagab, et nendes RNA molekulides peitunud kahjulik sõnum jääks valkudele edastamata. Aga selle eesmärgini on võimalik jõuda ka oligonukleotiididel põhinevate kunstlike ensüümidega, mis suudavad iseseisvalt RNA molekulid lõhustada, sõltumata looduslikest ensüümidest ning nendega kaasnevatest piirangutest.

Selle doktoritöö eesmärk oli seesuguste kunstlike ensüümide arendamine. Põhinedes peptiidnukleiinhappel (PNA) – sünteetilisel DNA analoogil, olid need kunstensüümid (PNAsüümid) varustatud nii-nimetatud „molekulaarsete kääridega“, et võimaldada RNA molekulide „katki lõikamine“.

Oligonukleotiididel põhinevate kunstensüümide potentsiaal ravimikandidaatidena sõltub sellest, kui kiiresti nad RNA märklaudu suudavad lagundada, nende täpsusest lagundada ilmtingimata ainult soovitud RNA sihtmärk ning sellest, kas nad suudavad aktiivsuse säilitada füsioloogilises keskkonnas. Varasemalt on arendatud erinevaid tüüpe oligonukleotiididel põhinevaid kunstlikke RNA-d lõhustavaid ensüüme, kuid enamasti on nende probleemiks aeglane reaktsioonikiirus ja mõnel juhul ka sõltumine metalliioonidest, mida bioloogises keskkonnas ei leidu.

Selles doktoritöös uuriti lähemalt juba varasemalt arendatud PNAsüüme, mille võime efektiivselt RNA-d lagundada nõuab vaseioonide kohalolu. Luubi all oli nii RNA ja PNAsüümi ehitusblokkide järjestus kui ka erinevate kriitiliste keemiliste muudatuste mõju, mille tulemusel koorusid välja mitmed huvitavad tähelepanekud kunstensüümide võimekusest. Need PNAsüümid on äärmiselt efektiivsed, kuid kuna vask ei esine vabalt bioloogilistes keskkondades, on nende kunstensüümide tulevik võimalik peamiselt tööriistadena teadustöös.

Tsink on bioloogiselt oluline metall, mida leidub inimese rakkudes. Seetõttu on tsink märksa atraktiivsem kunstensüümi kofaktor, kuid seni arendatud tsingil põhinevad RNA-d lõhustavad kunstensüümid on olnud madala võimekusega. Selles doktoritöös arendati tsingist sõltuvaid PNAsüüme, mille koostisesse kuuluvad uut tüüpi „molekulaarsed käärid“ ning mille aktiivsus on kõrgem kui isegi parimatel vasel põhinevatel PNAsüümidel varasemalt. Need tsink-PNAsüümid suudavad lõhustada pooled oma RNA sihtmärkidest kõigest 10 minutiga, olles seejuures väga täpsed ja lõigates iga RNA molekuli vaid ühest ja samast lõikekohast igas molekulis. Nende PNAsüümide ehitusblokkide järjestus on määrava tähtsusega, muutes need kunstensüümid väga täpseks. Samas on võimalik teatud osa nende järjestusest valida vastavalt haigustega seotud RNA sihtmärgile ning seega saab nende PNAsüümide abil efektiivselt hävitada erinevaid meditsiinilise tähtsusega RNA järjestusi.

Kunstensüümidel võib tulevikku olla nii geneetiliste kui ka parasiitide või viiruste põhjustatud haiguste ravis, kuna neid on võimalik suunata parasiitide või viiruse geneetilist informatsiooni lagundama, jättes inimese RNA puutumata. Meie tsink-PNAsüümid lõhustasid edukalt RNA mudeleid, mis olid loodud malaaria parasiidi ja SARS-CoV-2 koroonaviiruse geneetilise informatsiooni põhjal. Üks tähtis aspekt tsink-PNAsüümide puhul on vajadus tagada piisav tsingikontsentratsioon neid ümbritsevas keskkonnas. Huvitava kokkusattumusena on tsink vajalik ka malaaria parasiidi elutsüklis, mistõttu on tsingitase malaariaga nakatanud punavereliblede äärmiselt kõrge, tagades piisavalt vabu tsingiioone, et PNAsüümi tegevust toetada. Meditsiinilise tähtsusega RNA mudelite efetiivne lagundamine tsink-PNAsüümide poolt on lootust andev areng ning järgmise sammuna tuleks uurida PNAsüümide aktiivsust bioloogilises keskkonnas.

ABSTRACT

Synthetic modified oligonucleotides are gaining momentum as powerful therapeutic tools used in the treatment of life-threatening diseases. Degradation of disease-related RNA sequences is one of the goals achieved with oligonucleotide therapeutics, albeit the currently available technologies rely on the recruitment of endogenous enzymes, RNase H or RISC, limiting the chemical architecture of oligonucleotide drugs. Artificial ribonucleases based on conjugates of oligonucleotide analogues can be equipped with so-called "molecular scissors" to achieve catalytic RNA cleavage independently of endogenous enzyme action. If such artificial enzymes can be developed to a state where they accomplish rapid sequence-specific RNA cleavage under biological conditions, they could expand the arsenal of oligonucleotide-based tools available for nucleic acid manipulation for biological intervention.

Previously published Cu^{2+}-neocuproine conjugates of peptide nucleic acid (PNA) are efficient site-specific artificial enzymes (PNAzymes) that degrade RNA bulges of 4 nucleotides in length. In this thesis, the activity of these Cu^{2+} PNAzymes was probed further by studying the dependence of the cleavage rate on the length and composition of the RNA bulge. Reduction in the bulge length resulted in significantly slower cleavage rates for 3-nucleotide bulge-forming RNA targets. Moreover, the fast cleavage of 4-nucleotide bulges was shown to require critical functional groups – the exocyclic amino group and the 2'-hydroxyl group of the adenosine nucleotide at the cleavage site, and the PNAzyme was shown to necessarily require a chelating group as part of its structure. Finally, RNA cleavage rates were shown to be unaffected by elongation of the RNA/PNAzyme complex.

While Cu^{2+}-dependent PNAzymes could be impactful as research tools, they offer less hope for clinical applications due to the absence of free copper ions in biological fluids. As a more biocompatible alternative, Zn^{2+} is a desirable cofactor for artificial enzymes, although the previously published examples of such artificial enzymes have suffered from low activity. In this thesis, novel Zn^{2+}-dependent dimethyl-dipyridophenazine-based PNAzymes were developed. The dependence of their activity on the RNA bulge sequence, pH and Zn^{2+} ion concentration was studied in detail. These Zn^{2+} dimethyl-dppz PNAzymes cleaved 3-nucleotide bulge-forming RNA target sequences at a single site with down to 10-minute half-lives at pH 7.4, thus outperforming all previously published artificial ribonucleases. Moreover, they were shown to be capable of cleaving clinically relevant RNA sequences, namely a *Plasmodium falciparum* (malaria parasite) mRNA model and a SARS-CoV-2 genomic RNA model.

The sequence of the RNA target was shown to be highly significant, both in the single-stranded bulge region and in the hybridised bulge-closing regions on both sides. The cleavage of 2, 3 and 4-nucleotide RNA bulges by Zn^{2+} dimethyl-dppz PNAzymes was studied and the sequence requirements for efficiently cleaved RNA targets were identified. The unprecedented efficiency and specificity of Zn^{2+} dimethyl-dppz PNAzymes will hopefully inspire future investigations to assess their efficacy in biological settings.

LIST OF SCIENTIFIC PAPERS

I. **Olivia Luige**, Merita Murtola, Alice Ghidini and Roger Strömberg. Further Probing of Cu^{2+}-Dependent PNAzymes Acting as Artificial RNA Restriction Enzymes. *Molecules*, 2019, 24, 672.

II. **Olivia Luige**, Partha Pratim Bose, Rouven Stulz, Peter Steunenberg, Omar Brun, Shalini Andersson, Merita Murtola and Roger Strömberg. Zn^{2+}-Dependent peptide nucleic acid-based artificial ribonucleases with unprecedented efficiency and specificity. *Chem. Commun.*, 2021, 57, 10911-10914.

III. **Olivia Luige**, Kristina Karalė, Partha Pratim Bose, Martin Bollmark, Ulf Tedebark, Merita Murtola and Roger Strömberg. Influence of sequence variation on the RNA cleavage activity of Zn^{2+}-dimethyl-dppz-PNA-based artificial enzymes. *RSC Advances*, 2022, 12, 5398-5406

PUBLICATIONS NOT INCLUDED IN THE THESIS

I. François Halloy, Annabelle Biscans, Katherine E. Bujold, Alexandre Debacker, Alyssa C. Hill, Aurélie Lacroix, **Olivia Luige**, Roger Strömberg, Linda Sundstrom, Jörg Vogel, Alice Ghidini. Emerging Technologies and Innovative Developments in RNA Therapeutics. *RNA Biology*, 2022, Accepted for publication

CONTENTS

LIST OF ABBREVIATIONS

A	adenosine (or adenine)
Ac	acetyl
ACE	bis(2-acetoxyethoxy)methyl
ASO	antisense oligonucleotide
aq	aqueous
Bhoc	benzhydryloxycarbonyl
Boc	*tert*-butyloxycarbonyl
C	cytidine (or cytosine)
CD	circular dichroism spectroscopy
CE	cyanoethyl
CPP	cell-penetrating peptide
EMA	European Medicines Agency
FDA	U.S. Food and Drug Administration
Dap	diamino-propionic acid
DCM	dichloromethane
DIC	*N,N'*-diisopropylcarbodiimide
DMD	Duchenne muscular dystrophy
DMSO	dimethyl sulfoxide
DMT(r)	dimethoxytrityl
DNA	deoxyribonucleic acid
dppz	dipyridophenazine
EDTA	ethylenediaminetetraacetic acid
ESI-MS	electrospray ionisation mass spectrometry
EXP1	*Plasmodium falciparum* exported protein 1
Fmoc	9-fluorenylmethoxycarbonyl
G	guanosine (or guanine)
GalNAc	N-acetylgalactosamine
HATU	1-[Bis(dimethylamino)methylene]-1H-1,2,3-triazolo[4,5-b]pyridinium 3-oxide hexafluorophosphate
HEPES	4-(2-hydroxyethyl)-1-piperazineethanesulfonic acid
HPLC	high pressure liquid chromatography
HRMS	high resolution mass spectrometry
IE(X)-HPLC	ion-exchange HPLC
LNA	locked nucleic acid
MALDI-MS	matrix-assisted laser desorption/ionisation mass spectrometry
m-BCR/ABL	major brakepoint cluster region/ Abelson tyrosine kinase
Me	methyl
MOE	methoxy-ethyl
miRNA	microRNA

mRNA	messenger RNA
Mtt	4-methyltrityl
NMM	*N*-methyl morpholine
NMP	*N*-methyl-2-pyrrolidone
NMR	nuclear magnetic resonance spectroscopy
OBAN	oligonucleotide-based artificial nuclease
ON	oligonucleotide
PMO	phosphorodiamidate morpholino oligomer
PNA	peptide nucleic acid
PNAzyme	peptide nucleic acid-based artificial enzyme
pre-mRNA	precursor mRNA
Ph	phenyl
PS	phosphorothioate
POC	peptidyl-oligonucleotide conjugate
Pu	purine
Py	pyrimidine
Qtof MS	quadrupole time-of-flight mass spectrometry
RISC	RNA-induced silencing complex
RNA	ribonucleic acid
RNase H	Ribonuclease H
RNAi	RNA interference
RP HPLC	reversed phase HPLC
SARS-CoV-2	severe acute respiratory syndrome coronavirus 2
SCoV2-PLpro	SARS-CoV-2 betacoronavirus papain-like protease
siRNA	small interfering RNA
SMA	spinal muscular atrophy
SSO	splice-switching oligonucleotide
T	thymidine (or thymine)
TBDMS	*tert*-butyl(dimethyl)silyl
TEAA	triethylammonium acetate
U	uridine (or uracil)

1 INTRODUCTION

Deoxyribonucleic and ribonucleic acids (DNA and RNA) are fundamental biomolecules that perform complex biological functions, including the storage of genetic information and enabling of protein production. Due to their key role in critical biological processes, abnormalities present in nucleic acids can translate to abnormalities in proteins, which can in turn have profound adverse effects on fundamental processes in the body.

Traditional therapeutic interventions rely on targeting a rather limited set of proteins, mostly enzymes or receptors,[1,2] using small-molecule drugs. These conventional drugs act by "lock and key" type interactions by binding to specific binding pockets present in their target proteins.[2,3] However, not all potential drug targets contain such surfaces, particularly when the therapeutic strategy is to interfere with harmful protein-protein interactions, where the targets would be large protein surfaces.[2–4] As such, targeting the protein interactome using traditional low-molecular weight drugs is notoriously challenging, and therefore the extent of drug targets that are traditionally considered "druggable" is rather limited.[1,2,5]

Aside from using proteins as drugs targets, it is possible to silence erroneous genetic information by targeting specific DNA or RNA sequences with drugs analogous to DNA and RNA, and thus modulate or prevent the production of certain proteins.[3,6] Such analogues are called therapeutic oligonucleotides; they are short synthetic modified nucleic acid molecules that take advantage of the intrinsic affinity and molecular recognition between complementary nucleic acids.

Figure 1. The central dogma of molecular biology. The flow of information from DNA to RNA through transcription, and from RNA to protein through translation.

The promise of oligonucleotide therapeutics has motivated research for decades. The central dogma of molecular biology describes the flow of genetic information from DNA to RNA to proteins (Fig 1).[7,8] Oligonucleotides can interfere with the passage of information between these biomolecules, giving them enormous potential as therapeutic agents.[3,9] After 30 years of clinical development, the oligonucleotide therapeutics field has enjoyed significant success in recent years. Amid numerous ongoing clinical trials, several oligonucleotide drugs have been approved in the U.S. and Europe,[3,10–13] giving long-awaited hope to patients suffering from debilitating genetic diseases.

2 LITERATURE REVIEW

2.1 Synthetic modified oligonucleotides

Therapeutic oligonucleotides are short synthetic modified oligonucleotides – analogues of naturally occurring DNA and RNA molecules. The principal challenge with therapeutic oligonucleotides is giving them "drug-like" properties, as they need to be resistant to enzymatic degradation, exhibit enhanced binding affinity compared to natural nucleic acids, and have enhanced bioavailability and cellular trafficking properties.[14,15] As such, numerous chemical modifications to the natural phosphodiester linkages, the ribose sugar moiety and nucleobases have been developed.[3,14,15] Moreover, the properties of oligonucleotides can be further improved by conjugating them to targeting ligands or other molecular entities (*e.g.* carbohydrates, lipids or peptides).[16–20]

A particular advantage of oligonucleotide drugs is that the delivery and potency of an oligonucleotide drug relate to its chemical design, while the target is determined by the nucleobase sequence, hence the two can be optimised somewhat separately.[3,14] Once the chemical structure and the delivery strategy of an oligonucleotide drug have proved effective in a particular tissue, this success is likely to translate between different targets and therefore diseases affecting the same tissue.[14]

Therapeutic oligonucleotides typically contain a variety of chemical modifications, including backbone, 2'-ribose and nucleobase modifications.[3,14,15] The phosphodiester-sugar backbone of naturally occurring nucleic acids (Fig 2a) is rapidly degraded by enzymes, and its polyanionic character is responsible for their poor cellular uptake. As such, there has been a long-standing desire to modify the natural backbone, leading to numerous modifications. The most common modification is the replacement of phosphodiesters (PO) with phosphorothioate (PS) linkages (Fig 2b), which provides nuclease stability and enhanced uptake through increased serum albumin binding.[3,15] Among uncharged backbones that have been developed, two have found widespread use, both of which are resistant to degradation by nucleases and provide increased binding affinity to nucleic acids.[21–23] These modifications are a heterocyclic phosphorodiamidate morpholino (PMO) modification (Fig 2c) and peptide nucleic acid (PNA) (Fig 2d), which contains a "pseudopeptide" backbone composed of N-(2-aminoethyl)glycine units.[3,14,17,24,25] The PNA backbone was designed to be structurally homomorphous to the DNA backbone,[26] and it has been shown to mimic nucleic acids by forming strong double helices with DNA and even more so with RNA.[27]

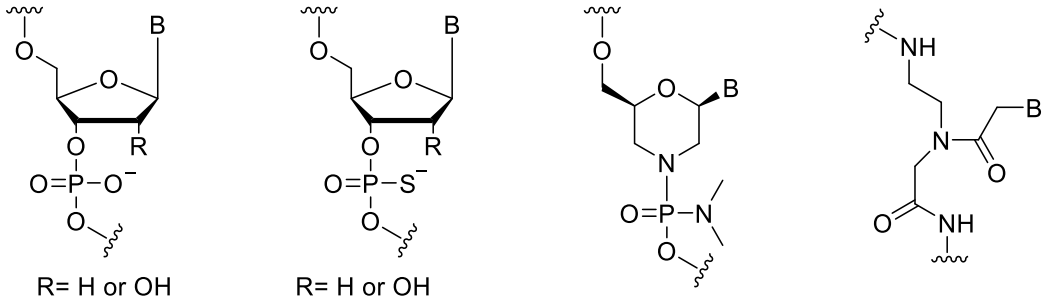

Figure 2. Phosphodiester backbone modifications in synthetic oligonucleotide analogues

The most common modifications to the sugar include 2'-*O*-methyl (Fig 3a), 2'-methoxyethyl (Fig 3b) and 2'-fluoro (Fig 3c) ribose modifications, which also improve the nuclease stability of oligonucleotides.[15,23] Moreover, 2'-bridged nucleic acids, namely locked nucleic acids containing a 2',4'-methylene linkage (LNA) (Fig 3d) and 2',4'-constrained ethyl nucleic acid (cET) (Fig 3e) provide significantly enhanced affinity by locking the sugar pucker into the C3'-endo conformation.[15,28] Finally, several nucleobase modifications, including the use of 5-methyl cytosine, have led to an increase in duplex stability.[3]

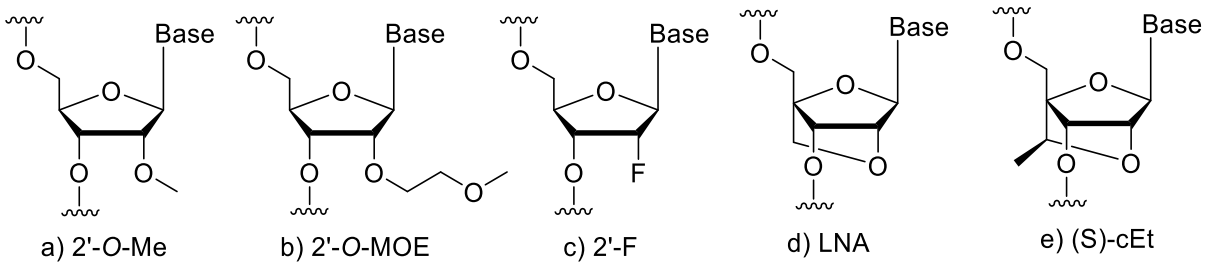

Figure 3. Ribose modifications in synthetic oligonucleotide analogues

2.2 Mechanisms of oligonucleotide therapeutics

Therapeutic oligonucleotides can be designed to perform various tasks by a range of mechanisms of action. In fact, the chemical design of an oligonucleotide drug is largely influenced by its mechanism, as the types and patterns of chemical modifications must be compatible with the desired action.

The classical and one of the most important classes of oligonucleotide drugs is antisense oligonucleotides (ASOs; Fig 4.A). ASOs bind to their RNA targets by Watson-Crick base pairing and thereafter either sterically block translation or splicing, or mark the RNA for enzymatic degradation.[3,14,15,29] The latter (Fig 4.Ai) allows for the reduction of harmful RNA levels via recruitment of an endogenous enzyme, a Mg^{2+}-dependent endoribonuclease called RNase H, which recognises DNA/RNA heteroduplexes and hydrolyses the RNA strand in a sequence non-specific fashion.[30–32] The principal structural demand for the RNase H-mediated RNA cleavage mechanism is that the synthetic antisense oligonucleotides must contain a stretch of deoxyribose nucleotides, capable of forming a heteroduplex with the RNA target, which serves as a substrate for the enzyme. These DNA nucleotides can contain phosphorothioate linkages,[14] offering some protection against enzymatic degradation as well as improved uptake and cellular trafficking properties. Moreover, these ASOs are typically designed as gapmers, where modified RNA nucleotides are included on either side of the central DNA gap region, rendering the oligonucleotides resistant to exonucleases and improving their binding affinity.[14,15]

As mentioned above, antisense oligonucleotides can also affect the intricate splicing process by which pre-mRNA is converted into mature mRNA in the nucleus prior to translation (Fig 4.Aii). In this case, it is important that they do not elicit RNase H action, but instead sterically block splicing factors and thereby modulate splicing.[3,15,33,34] Here, the precise binding sequence of the splice-switching oligonucleotide (SSO) is key, as splicing is carefully controlled by exon and intron regions in pre-mRNA. By sterically blocking the pre-mRNA splice sites (*i.e.* the pre-mRNA splice silencing or splice enhancing sequences), it is possible to

achieve exon inclusion or exon skipping, respectively.[34] The SSO/pre-mRNA complex must be unrecognisable for RNase H and the SSO must therefore consist of fully 2'-ribose-modified phosphorothioate oligonucleotides or fully modified backbones such as morpholinos[15,33,34] or PNA.[35–37]

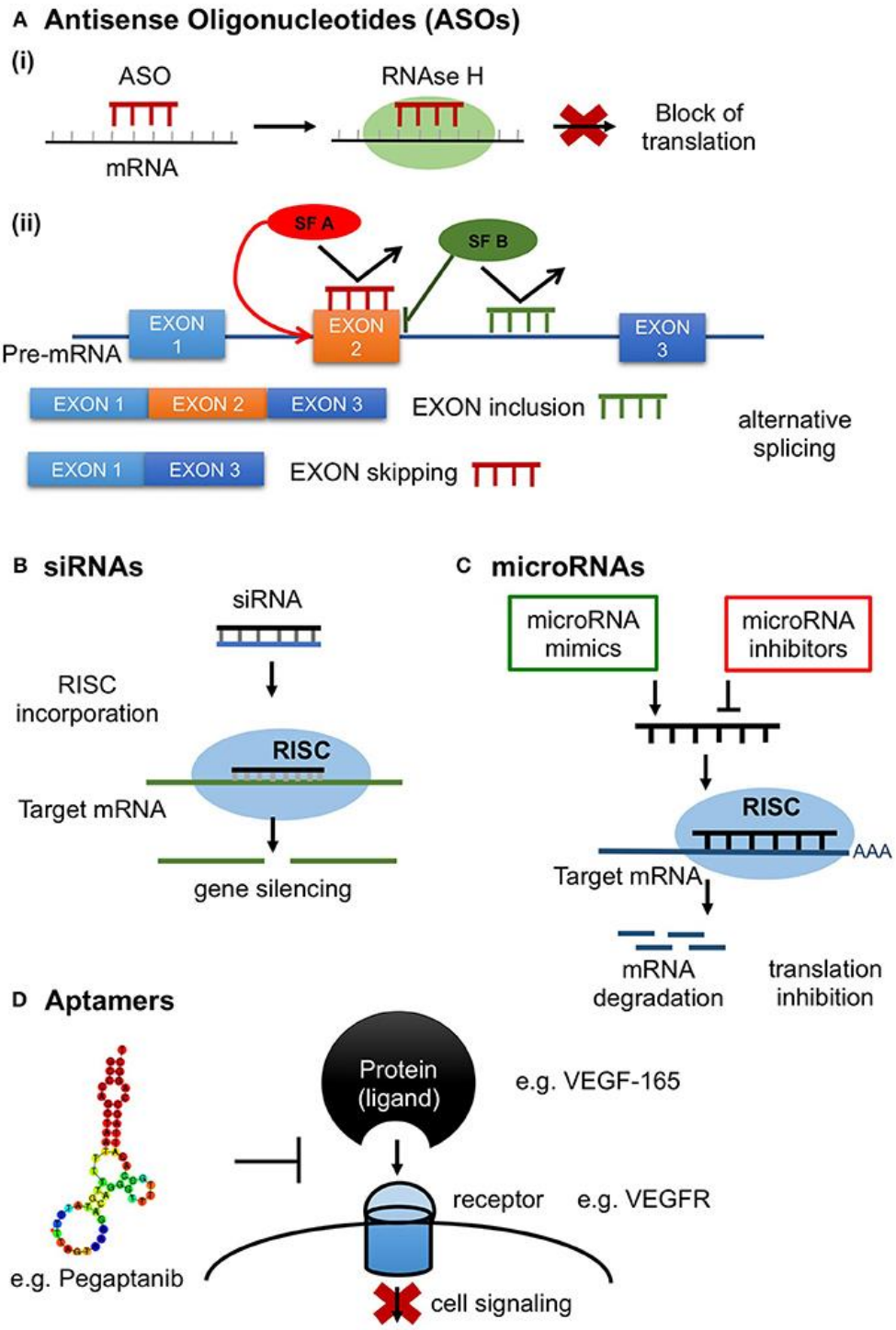

Figure 4. Mechanisms of oligonucleotide therapeutics. A. Antisense oligonucleotides (ASOs) that modify protein production by either (Ai) triggering RNase H-mediated mRNA cleavage or (Aii) blocking pre-mRNA splicing sites to redirect alternative splicing. B. Small interfering RNAs (siRNAs) that recruit the RISC complex to induce mRNA cleavage. C. microRNA mimics and inhibitors that modify gene expression. D. Aptamers that bind to targets by complex shape-dependent interactions. Reprinted from Laina *et al*, *Front. Physiol*., 2018, 9, 953.[29]

Another important class of oligonucleotide therapeutics is small-interfering RNAs (siRNAs; Fig 4.B).[3,15,38] This therapeutic approach relies on double-stranded RNA molecules that utilise the RNA interference (RNAi) pathway to inhibit gene expression – a discovery for which Andrew Z. Fire and Craig C. Mello were jointly awarded the Nobel Prize in Physiology and Medicine 2006.[39] One of the strands in siRNA (the guide strand) associates with Argonaute among other proteins to form the RNA-induced silencing complex (RISC), which then degrades the complementary RNA target.[38,40] Unique design requirements apply to these double-stranded oligonucleotides that rely on the endogenous RNAi pathway. For example, their design must create a thermodynamic bias towards the loading of the guide strand into the RISC complex as opposed to the passenger strand.[14,41] Moreover, the pattern and extent of chemical modifications tolerated in siRNAs are more complex,[14,42] but similarly to the antisense approaches described above, 2'-*O*-Me, 2'-F sugar and PS backbone modifications have also found use in siRNAs.[14,38] Moreover, as a laboratory tool for manipulating gene expression siRNA has several advantages compared to ASOs and has therefore found wide-spread use in molecular biology.[15]

Oligonucleotides can be used to target a variety of different classes of RNA.[3,33,43] Messenger RNA (mRNA) transcripts are directly translated to proteins, and hence targeting mRNA or pre-mRNA provides a straightforward path to blocking or enabling protein synthesis. Nonetheless, non-coding RNAs, such as microRNAs (miRNA), have a significant role in controlling gene expression. Oligonucleotides can target miRNA (in which case they are called anti-miRs) to modulate gene expression by sterically blocking miRNA, or they can target mRNA by acting as miRNA mimics (Fig 4.C).[3,29] In addition, double stranded DNAs can be used as DNA decoys to sequester transcription factors, and there are also RNA-cleaving DNAzymes.[3] Moreover, the interactions between the oligonucleotides and their targets can be more complex than hybridisation-driven base-pairing. Aptamer drugs are nucleic acids evolved through *in vitro* selection of functional nucleic acids, which can target proteins by more complex molecular interactions (Fig 4.D).[29,44]

2.3 Approved oligonucleotide-based therapeutics

The ability of a synthetic antisense oligonucleotide to inhibit protein translation was first demonstrated by Paul Zamecnik and Mary Stephenson in 1978.[45,46] The first antisense drug fomivirsen (Vitravene) was approved by the FDA in 1998 for the treatment of cytomegalovirus retinitis.[13] However, the progress of the oligonucleotide therapeutic platform was initially slow. An aptamer drug pegatanib (Macugen) targeting the vascular endothelial growth factor (VEGF165) was approved for the treatment of neovascular age-related macular degeneration in 2004.[13,33] Nearly a decade later, mipomersen (Kynamro) – an antisense drug for the treatment of homozygous familial hypercholesterolaemia – was approved by the FDA in 2013, although not by the EMA due to concerns regarding adverse cardiovascular events.[13] Defibrotide (Defitelio) is another oligonucleotide-based drug with a complex non-specific mechanism approved in 2016 for the treatment of severe hepatic veno-occlusive disease.[13]

Despite the early setbacks and failed clinical trials,[14,33,47] advances in chemical modifications and delivery strategies have led to significant clinical success in recent years.[12,18,48,49] Oligonucleotide therapeutics have finally reached considerable clinical utility, resulting in a

number of approved drugs based on splice-switching oligonucleotides, RNase H-dependent gapmer ASOs as well as siRNA.[10,12]

Splice-switching oligonucleotide nusinersen (Spinraza) that restores protein synthesis by exon inclusion was approved by the FDA in 2016 for the treatment of spinal muscular atrophy (SMA).[3,13,34] An exon-skipping splice-switching oligonucleotide eteplirsen (Exondys 51) was approved in 2016 for the treatment of Duchenne muscular dystrophy (DMD).[3,13,34] Since then, three more exon-skipping therapies have been approved for DMD. Golodirsen (Vyondys 53) gained accelerated FDA approval in late 2019,[49,50] viltolarsen (Viltepso) was first approved in early 2020 in Japan,[51,52] and casimersen (Amondys45) gained approval early 2021 in the U.S.[53] Moreover, a step towards truly personalised medicine was an investigational exon-skipping drug Milasen, designed and developed in 2017 and approved in early 2018 for the urgent treatment of a single patient with a rare genetic disease.[54]

Inotersen (Tegsedi) is an RNase H-dependent gapmer ASO, and patisiran (Onpattro) an siRNA in a lipid nanoparticle, which were both approved by the FDA for the treatment of hereditary transthyretin amyloidosis in 2018.[55,56] Volanesorsen (Waylivra) is an RNase H-dependent triglyceride-lowering drug for the treatment of a rare genetic condition called familial chylomicronemia syndrome approved in Europe in 2019.[49,57] Givosiran (Givlaari) is an siRNA drug and the first GalNAc conjugate approved for the treatment of acute hepatic porphyria (AHP) in late 2019.[58] A cholesterol-lowering drug inclisiran (Leqvio) that reduces PCSK9 production[59,60] is another GalNAc-siRNA conjugate approved in Europe in late 2020,[61,62] and in the U.S. in late 2021. Another GalNAc-siRNA conjugate lumasiran (Oxlumo) was approved in late 2020 both in Europe and in the U.S for the treatment of primary hyperoxaluria.[63]

The approval of inclisiran is particularly significant, due to the major role of low-density lipoprotein cholesterol (LDL-C) in the development of cardiovascular disease which is a leading cause of mortality globally.[61] As such, oligonucleotide therapeutics are clearly advancing towards the treatment of broader diseases and not just rare genetic disorders, although it should be noted that the latter can greatly benefit from the so-called "orphan drug" designation.[64]

2.4 Oligonucleotide delivery

Oligonucleotide delivery to the desired tissue, cellular uptake as well as endosomal escape and delivery to the intracellular site of action are complex challenges that have been major obstacles for oligonucleotides in a therapeutic context.[17,25,48,65] The goal of targeted delivery is to achieve higher concentrations of the drug in the target tissue and subcellular compartment, which can enhance the therapeutic potency, while also reducing toxicity by lowering the concentration of the drug in other tissues.[17,66] Moreover, this can enable lower doses to be administered, which alleviates the high cost associated with oligonucleotide therapeutics.[66]

Many strategies are being developed to tackle the delivery challenges. These include chemical modifications, as cellular uptake of naked oligonucleotides is facilitated by incorporation of LNA and PS modifications.[48] Moreover, promising targeted delivery approaches explore conjugation to lipids (*e.g.* cholesterol), cell-targeting or cell-penetrating peptides, antibodies, aptamers or sugars (*e.g.* GalNAc), formulation with lipid nanoparticles (LNPs) as well as exosome-mediated delivery.[17,48,66] For example, receptor-mediated targeting approaches[48] and

conjugation to arginine-rich peptides[49] are being explored to increase delivery to the muscle, as the currently approved SSOs for the treatment of DMD are intravenously administered unconjugated PMOs that show relatively low levels of exon skipping.[49,50,52,53]

Efficient delivery to the liver has been achieved upon systemic (intravenous or subcutaneous) administration of many oligonucleotides,[3] as is the case for the subcutaneously administered inotersen.[17,55,67] Lipid nanoparticles have been used for targeted delivery into the liver,[66] as exemplified by patisian.[56] Moreover, conjugation of oligonucleotides to N-Acetyl-D-galactosamine (GalNAc), which is a ligand for the asialoglycoprotein receptor abundant in hepatocytes, has been a recent breakthrough, resulting in increased uptake into the hepatocytes of the liver.[18,66] However, extra-hepatic delivery remains a substantial challenge.[17,48,68]

Local delivery has been behind the success of several oligonucleotide therapies. The first approved oligonucleotide drugs fomivirsen and pegatanib were delivered locally to the eye via intraocular injection directly into the vitreous humor.[13] Moreover, efficient local delivery of single stranded oligonucleotides to the central nervous system has been achieved via direct intrathecal injection (into the cerebrospinal fluid),[3,25,43] including in the case of nusinersen and milasen.[13,54]

2.5 Degradation of RNA

The ability to trigger enzymatic degradation of mRNA using synthetic oligonucleotides relies on the fundamental importance of enzymatic RNA cleavage in nature. In fact, there are numerous endogenous enzymes tasked with degrading foreign or unneeded RNAs.[69,70] Such enzymes can operate in the absence of metal ions or they can be dependent on a metal co-factor, such as Mg^{2+}, Ca^{2+} or Co^{2+} ions.[71] Examples of RNA-cleaving enzymes include ribonucleases RNase A and RNase H as well as the RNA-induced silencing complex (RISC). In addition to protein enzymes, there are also endogenous catalytic nucleic acids, such as hammerhead and hairpin ribozymes, accompanied by their laboratory-made colleagues like DNAzymes, capable of catalysing the cleavage of phosphodiester bonds in a site-specific manner.[70,72]

In the absence of a catalyst, the nucleic acid phosphodiester backbone is stable under physiological conditions. Based on extrapolation from studies using model compounds, the half-life for phosphodiester hydrolysis at 25 °C is estimated to be in the range of 30 million years in DNA and at least 10 years in RNA.[73] This predisposition for cleavage in RNA is due to the presence of the 2'-hydroxyl group, an intramolecular nucleophile that can attack the phosphorus of the vicinal 3'-phosphodiester linkage, followed by the departure of the 5'-oxyanion, leading to the 2',3'-cyclic phosphate product.[74] A general base catalyst deprotonates the nucleophile and a general acid catalyst protonates the 5'-leaving group.[69] The conformation of the participating groups is critical, and the adoption of a “near-attack” or “in-line” conformation (where the 2'-hydroxyl nucleophile, the phosphorus atom and the 5'-leaving group form a 180° angle) facilitates the transesterification reaction (Fig 5).[71,74] Consequently, RNA is more readily cleaved in a single strand,[69] or in unpaired bulge regions formed within the double helical structure, where the cleavage site nucleotides have the freedom to adopt a variety of conformations.[71] Alternatively, instead of the 2'-hydroxyl, external nucleophiles can sometimes be used for RNA cleavage (as for DNA cleavage), including water and amino acid side chains such as serine, tyrosine and histidine.[69,73]

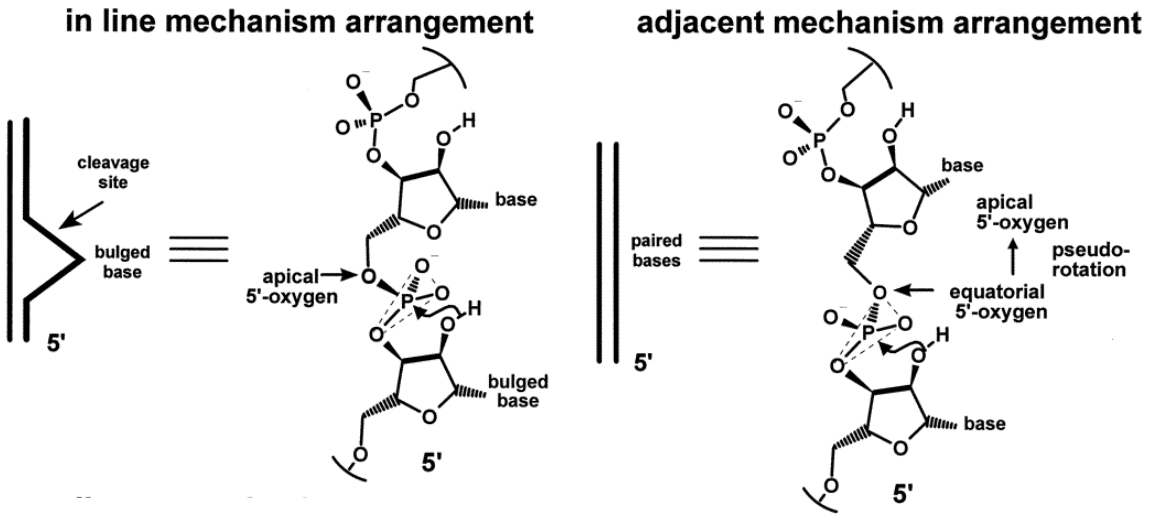

Figure 5. Cleavage site in a single-stranded bulge region allowing for an "in-line" or "near attack" alignment, where the 2'-hydroxyl nucleophile, the phosphorus atom and the 5' leaving group form a 180° angle (left) versus fully complementary double-stranded RNA arrangement, where pseudorotation of the 5'-oxygen from the equatorial to the apical position is required before cleavage at the P-5'-O bond can occur (right). Reprinted (adapted) with permission from Hüsken *et al*. *Biochemistry* 1996, 35, 51, 16591–16600. Copyright 1996 American Chemical Society.[71]

For example, one of the most studied ribonucleases RNase A cleaves single stranded RNA substrates using two histidine residues in its catalytic site, while not requiring a metal co-factor.[75] The general acid-base catalysis involves the ribose 2'-hydroxy intramolecular nucleophile while the two histidine residues provide an imidazolium ion that deprotonates the nucleophile and an imidazole that protonates the 5' leaving group.[70,75] Furthermore, the ammonium group of a lysine residue is used to stabilise the negative charge on the non-bridging oxygen of the phosphoryl group in the transition state.[72,75] On the other hand, RNase H is a Mg^{2+}-dependent ribonuclease that cleaves DNA/RNA hybrid double strands by making use of a deprotonated water molecule to perform an in-line nucleophilic attack on the phosphorus, followed by protonation of the leaving group by another water molecule.[76] Furthermore, the cleavage of double stranded RNA by the RNA-induced silencing complex (RISC) relies on a protein called Argonaute 2, which has been shown to be structurally similar to RNase H, containing a critical tetrad of carboxylate-containing amino acids in its catalytic site to position the Mg^{2+} ions.[41]

When the above-mentioned enzymes are utilised for clinical or scientific purposes, the synthetic oligonucleotide must be compatible with the corresponding enzyme action. For one, this means that a significant deoxyribose or ribose character must be preserved and thus PMO and PNA modifications are not themselves compatible, nor do their backbone chemistries make them suitable for straightforward inclusion in mixmer oligonucleotides. Different design requirements apply for siRNAs and gapmer ASOs, but in general chimeric oligonucleotides with a combination of different modifications are required.[14,15]

A key aspect is the ability for one synthetic oligonucleotide to act on several RNA targets, thus giving turnover of the substrate. This catalytic mode of action allows for the oligonucleotides to become much more efficient, which makes the drugs more potent, alleviating problems associated with the high cost and difficult delivery. For example, single-stranded RNase H-

dependent ASOs must have a high enough binding affinity to their target to compete with RNA binding proteins or RNA secondary structures. This results in the need for a delicate balance, as in addition to requiring sufficiently strong binding affinity to act in the first place, the synthetic oligonucleotide must also have a sufficiently weak binding affinity to the RNA fragments to allow for dissociation after the target has been cleaved.[14] Thus, the design of the oligonucleotide is critical. When it comes to gapmer ASOs, shorter oligonucleotides containing modifications that confer high affinity such as LNA and cET have been shown to be more potent than longer oligonucleotides with lower affinity modifications.[14] However, the use of these more potent gapmer ASOs has also been shown to lead to the cleavage of RNAs that are not entirely complementary, *i.e.* off-targets, resulting in significant toxicity.[14,15]

2.6 Principles of oligonucleotide-based artificial ribonucleases

Synthetic oligonucleotides can themselves be transformed into artificial ribonucleases by equipping them with an intrinsic ability to catalytically cleave RNA.[77,78] First, such oligonucleotides bind to their target, utilising their sequence-specific recognition properties. Then, their dual action is realised by so-called "molecular scissors" embedded in their structure, which promote the cleavage of the bound target. Lastly, the cleaved fragments should be released so that the artificial ribonuclease finds the next target and the catalytic cycle can continue. Such artificial ribonucleases could be efficient therapeutics, while the chemistry of such oligonucleotide drugs would not be restricted to the same chemical design and modification requirements that apply to siRNAs and RNase H-dependent ASOs. Oligonucleotide-based artificial ribonucleases could thus expand the arsenal of molecular tools available for selective nucleic acid manipulation for biological intervention. In addition to such purely synthetic constructs, an alternative area of ongoing research is ribozyme mimics (*e.g.* xenonucleic acid enzymes (XNAzymes) such as 2'-fluoroarabino nucleic acid enzymes (FANAzymes)) generated through in vitro evolution.[79,80]

Artificial ribonucleases have the potential to become equal counterparts to some of the previously mentioned molecular tools with wide-ranging applications, but the key challenge is to achieve sufficiently high catalytic efficiency to allow for significant cleavage activity and thus meaningful reduction of RNA levels. The critical task is the selection and positioning of chemical moieties within oligonucleotides that can act as "molecular scissors" and catalyse the cleavage of phosphodiester linkages in RNA.[77,81] Such moieties are typically covalently conjugated to RNA recognition components such as nucleic acids (*e.g.* DNA),[82] their analogues (2'-*O*-Me RNA or PNA) or RNA-binding peptides.[77,78]

The "molecular scissors" can be based on catalytic arginine and leucine-rich peptides or oligoamines such as ethylenediamine and diethylenetriamine or imidazole moieties that can act as acid-base catalysts at physiological pH, similarly to the RNase A mechanism detailed above.[78] Moreover, metal ion-catalysed phosphodiester cleavage can be taken advantage of with oligonucleotides conjugated to chelating groups that coordinate metal ions. Among the catalytically active metals that promote phosphodiester hydrolysis in RNA are divalent transition metals such as Zn^{2+} and Cu^{2+} as well as alkaline earth metals, but notably even more so trivalent lanthanide ions such as Tm^{3+}, Yb^{3+} and Lu^{3+}.[78]

Metal-dependent artificial ribonucleases based on lanthanide ions such as Lu^{3+}, Eu^{3+}, La^{3+} and Dy^{3+} have been studied extensively.[81,83,84] Various macrocycles, including pyridine cyclophanes and texaphyrin, have been used as chelating agents, leading to RNA cleavage half-lives in the range of 2-3 h at pH 7.5 and 37 °C.[81,85] However, due to the lack of lanthanide ions in biological systems, such artificial ribonucleases have less potential as therapeutic oligonucleotides compared to Cu^{2+} and especially Zn^{2+}-based systems. Metal-dependent artificial ribonucleases containing Cu^{2+}-terpyridine complexes have shown half-lives down to 40 h at pH 7.5 and 37 °C, and even down to 5 h and less in the presence of the cooperative action of both 5'- and 3'-terminal oligonucleotide conjugates.[81,86] Moreover, more recent developments (discussed below) have focussed on neocuproine complexes which have shown particularly promising RNA cleavage activity in the presence of both Cu^{2+} and Zn^{2+} ions.[87–89]

Artificial ribonucleases benefit from a design where they are directed to cleave single-stranded RNA. These regions are more susceptible to cleavage than RNA double strands, as the latter would require a conformational change to achieve the required orientation of the 2'-hydroxyl, which would disrupt hydrogen bonding.[71] Cleavage at a single-stranded region of the RNA can be promoted when the catalytically active part of the artificial ribonuclease is placed at the terminus of the therapeutic oligonucleotide. This design has been commonly employed in the construction of artificial ribonucleases, but the key drawback here is the inability to release the target once the cleavage has occurred to allow for the binding of the next target.[82,90] Alternatively, the "molecular scissors" can be placed in a central position in the artificial ribonuclease, facing a stretch of unpaired bulged out nucleotides in the RNA, surrounded by complementary double strands. In this case the complex will become less stable as a result of cleavage and the cleaved RNA fragments will therefore dissociate more readily from the artificial ribonuclease.[77,81,82,89] As such, these artificial ribonucleases must force the formation of a single-stranded bulge region in the RNA target adjacent to the "molecular scissors" moiety.[71,77]

2.7 Recent progress in oligonucleotide-based artificial ribonucleases

Metal-free artificial ribonucleases are capable of cleaving their RNA targets without the assistance of metal cofactors and are therefore attractive due to their self-reliance. The design of various metal-free artificial ribonucleases has been inspired by the mechanism of RNase A, including those containing imidazole and trisbenzimidazole.[77,91]

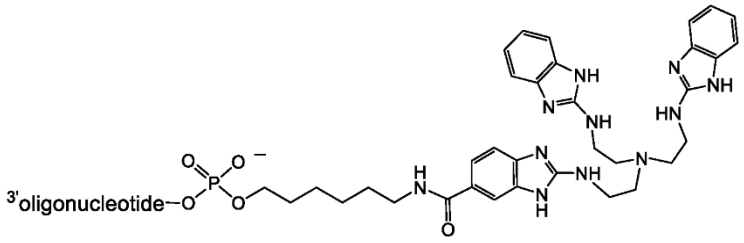

Figure 6. Structure of tris(2-aminobenzimidazole) attached to an oligonucleotide via a linker. Reprinted (adapted) from Zellmann *et al*, *Molecules,* 2019, 24(4), 807.[92]

Tris(2-aminobenzimidazole) conjugated to DNA, PNA or DNA/LNA mixmer backbones have been particularly effective metal-free artificial ribonucleases.[93–96] DNA and PNA conjugates of tris(2-aminobenzimidazole) (Fig 6) have been shown to cleave RNA site-specifically with approximately 11-20 h half-lives.[93,94,96] Moreover, the cleavage of RNA bulges by a centrally positioned "molecular scissors" moiety has enabled multiple substrate turnover.[96] Improved RNA cleavage half-lives down to 2.5-3.5 h have been recently reported with LNA/DNA mixmer oligonucleotides.[92,97] These artificial ribonucleases have been shown to cleave simple RNA models as well as more complex fragments of RNA transcripts from the 3'-UTR of proto-oncogenic serine/threonine kinase PIM1 mRNA.[92]

Catalytic peptides rich in arginine and leucine have been the "molecular scissors" of several types of peptidyl-oligonucleotide conjugates (POCs), including "dual" conjugates where the termini of the peptide are each conjugated to a separate oligonucleotide, as well as bulge-inducing conjugates.[91,98–101] The specificity of POCs contrasts that of other recently developed artificial ribonucleases, as in addition to the expected cleavage sites, they have been shown to cause RNA cleavage also at distant regions.[99,102,103] Achieving efficient turnover of the substrate has been a substantial challenge and POCs have been reported to rely on the recruitment of RNase H.[98,100] Nonetheless, recent report have indicated that the inclusion of two or three catalytic peptides instead of one in bulge-inducing POCs (Fig 7) increases their activity and enables 5-10-fold turnover of the RNA substrate.[103]

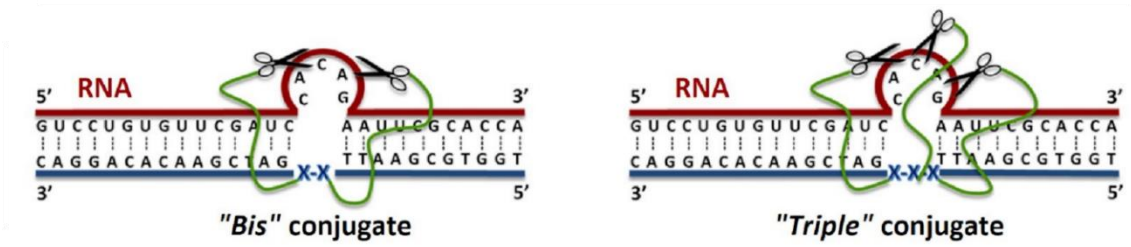

Figure 7. Schematic representation of bulge-inducing 'bis' (left) and 'triple' (right) peptidyl-oligonucleotide conjugates in complex with their RNA target (red), where the catalytic peptides are depicted as scissors linked to the oligonucleotide (blue) via aminohexyl linkers (green). Reprinted from Amirloo *et al*, *Nucleic Acids Research*, 2022, 50(2), 651–673.[103]

Zn^{2+} cofactor-dependent artificial enzymes based on neocuproine conjugates of 2'-*O*-Me oligonucleotides or PNA – OBANs and PNAzymes – have been developed.[87,90,104–107] As the second most abundant transition metal in the human body, zinc is a particularly desirable cofactor for artificial ribonucleases, as it is for many endogenous enzymes.[108,109] Zn^{2+}-neocuproine conjugates that take advantage of RNA bulge formation (Fig 8) have proven effective, albeit less efficient artificial ribonucleases than their Cu^{2+}-dependent counterparts.[87,89] The RNA cleavage rates are highly dependent on the length and sequence of the RNA bulge.[87,89,106,107] The earlier Zn^{2+}-dependent OBANs and PNAzymes cleaved a leukaemia-related bcr/abl mRNA transcript with down to 11 h half-lives at multiple sites in the 4-nucleotide RNA bulge.[105–107] More recently, down to 7-8 h cleavage half-lives have been demonstrated for the cleavage of 3 and 4-nucleotide bulges of preferred sequences with Zn^{2+}-neocuproine PNAzymes.[87]

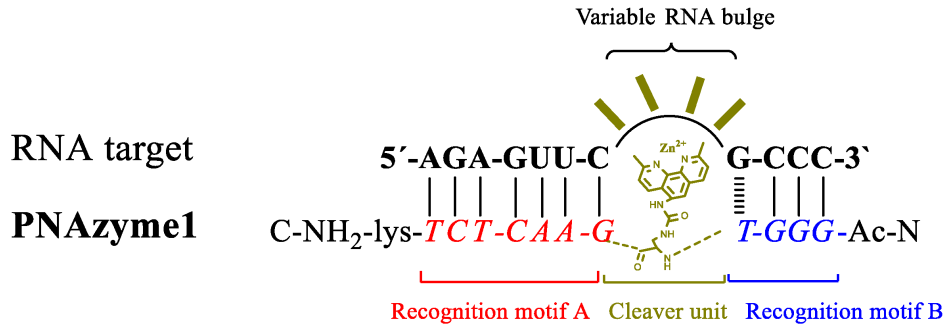

Figure 8. Complex between an RNA target and Zn^{2+}-neocuproine PNAzyme, where partial complementarity forces the formation of an RNA bulge at a position directly adjacent to the neocuproine "molecular scissors" moiety. Reprinted from Murtola *et al*, *Molecules* 2017, 22(11), 1856.[87]

Cu^{2+}-dependent PNA-neocuproine conjugates (PNAzymes) are capable of cleaving RNA with half-lives in the 20-30-minute range (Fig 9).[88,89] The cleavage is site-specific and highly dependent on the RNA bulge sequence with the highest rates observed for an AUAA bulge.[89] These PNAzymes exhibit excellent mismatch discrimination. Moreover, efficient turnover of a 100-fold excess of the RNA substrate has been demonstrated.[89] In addition, more complex clamping Cu^{2+}-neocuproine PNAzymes that form a triplex with the RNA target have been developed and can provide enhanced targeting properties.[88]

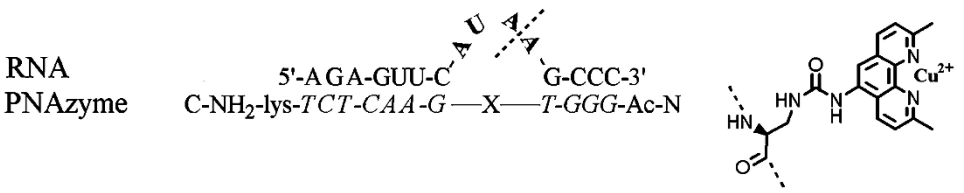

Figure 9. Reprinted (adapted) with permission from Murtola *et al*, *J. Am. Chem. Soc.* 2010, 132, 26, 8984-8990 Copyright 2010 American Chemical Society.[89]

In summary, prior to the work presented in this thesis, Cu^{2+}-dependent PNAzymes have unequivocally been the fastest artificial enzymes. The site- and sequence-specific nature of their action makes these PNAzymes promising as RNA restriction enzymes that can be used as research tools in molecular biology. However, their potential clinical applications are hindered by their reliance on Cu^{2+} ions, which are not available in cellular environments.[110] The metal-independent developments are intriguing due to their potentially greater biocompatibility, but their RNA cleavage activity is typically lower,[20,97,103] they depend on RNase H to achieve efficient action and turnover,[100] or they lack the ability to give turnover of the substrate.[101] As such, on the one hand, metal-free systems struggle to achieve efficient activity and turnover while constantly being outperformed by the metal-dependent artificial ribonucleases, which themselves lack inherent biocompatibility. This thesis aimed to provide a way forward for the field of artificial ribonucleases by developing PNAzymes that rely on more biocompatible Zn^{2+} ions, thus hoping to introduce the possibility of combining the excellent kinetics and turnover of the best metal-dependent artificial enzymes with the ability to retain the catalytic activity in biological settings.

3 RESEARCH AIMS

The overall research aim was to develop efficient artificial ribonucleases that could be of utility as research tools in molecular biology or as therapeutics to target endogenous disease-related RNA sequences for medical intervention. The studies undertaken towards this overarching research goal aimed to gain a deeper understanding of Cu^{2+}-neocuproine PNAzymes and to develop efficient biocompatible Zn^{2+}-dependent PNAzymes.

Paper I:

The aim was to gain a deeper understanding of Cu^{2+}-dependent PNA-neocuproine conjugates as artificial RNA restriction enzymes by studying their ability to cleave (1) 3-nucleotide RNA bulges, (2) RNA substrates with critical chemical modifications at the cleavage site, and (3) by investigating their catalytic performance in elongated RNA/PNAzyme complexes.

Paper II:

The aim was to develop novel biocompatible Zn^{2+}-dependent artificial ribonucleases by incorporating dimethyl-dipyridophenazine as "molecular scissors" in the PNAzyme structure. In addition, the research objectives were to characterise the RNA cleavage activity depending on the RNA bulge sequence, pH and Zn^{2+} ion concentration, and to demonstrate the cleavage of clinically relevant RNA target sequences.

Paper III:

The aim was to gain a deeper understanding of the significance of the RNA/PNAzyme sequence by studying the influence of sequence variation on the RNA cleavage activity of the Zn^{2+}-dependent dimethyl-dipyridophenazine PNAzymes. The sequence variations of interest were the bulge-closing base pairs in the (1) long recognition arm and (2) short recognition arm of the RNA/PNAzyme complex, (3) elongation of the short recognition arm sequence, and (4) variations in the 4-nucleotide bulge sequence among others.

4 MATERIALS AND METHODS

The full experimental details can be found in the Materials and Methods sections in papers I, II and III, but a summary of experimental descriptions is included below for clarity. All commercially available reagents and solvents were purchased as detailed in the experimental sections of papers I, II and III. RNA oligomers were either purchased purified and used as supplied, purified in-house by Merita Murtola according to established methods as detailed in the experimental sections of papers I, II and III, or synthesised by automated solid-phase synthesis by the author of this thesis, Rouven Stulz and Anders Dahlén, and purified by Rouven Stulz according to standard protocols detailed in paper II. Concentrations of RNA oligomers were determined by UV absorption at 260 nm on a Varian Cary 300 UV-Vis dual beam spectrophotometer (Varian, Palo Alto, CA, USA) and calculated from extinction coefficients obtained by the nearest neighbour approximation.[111]

4.1 Synthesis of peptide nucleic acid sequences

The synthesis of peptide nucleic acid (PNA) sequences was performed by conventional solid phase synthesis, using commercially available building blocks on an automated Biotage Initiator+ Alstra microwave peptide synthesis instrument.[112] The PNA sequences contained a lysine residue at the C-terminus for improved aqueous solubility,[24] and a centrally positioned Mtt-protected diamino-propionic acid (dap) for orthogonal attachment of the "molecular scissors" (*i.e.* the chelating moiety).[113] The syntheses were performed on Rink Amide resin (resulting in C-terminal amide) and the sequences were end-capped (acetylated N-terminus). The detailed synthesis protocol is summarised in papers I and II, but also described below for clarity.

The sequences were assembled automatically on Rink Amide ChemMatrix resin (0.47 mmol/g) on a 10 μmol scale in a 5 mL reactor vial using 9-fluorenylmethoxycarbonyl (Fmoc) chemistry under inert gas (N_2). Prior to commencing the synthesis cycles, the resin was allowed to swell in NMP for 20 min at 70 °C (microwave heating). The synthesis consisted of repeated cycles of Fmoc deprotection, coupling and capping steps as follows. Each synthesis cycle commenced with Fmoc deprotection by treating the resin with piperidine-NMP (1:4, *v/v*) twice (3 min and 10 min) at room temperature, followed by washing with NMP (×4). Couplings of commercially available PNA monomers (Fmoc-PNA-A(Bhoc)-OH, Fmoc-PNA-G(Bhoc)-OH, Fmoc-PNA-C(Bhoc)-OH and Fmoc-PNA-T-OH) or Fmoc-L-Lys(Boc)-OH or Fmoc-L-Dap(Mtt)-OH (4 equivalents, 0.2 M) were performed using DIC (0.2 M in NMP) and Oxyma (0.2 M in NMP) at 75 °C (microwave heating) over 6 min. After each coupling, the resin was washed with NMP (×4) and treated with NMP-lutidine-acetic anhydride (89:6:5, *v/v/v*) for 2 min, followed by washing with NMP (×4). Additionally, the final synthesis cycle included another Fmoc deprotection step and an NMP-lutidine-acetic anhydride capping step to achieve the end-capped PNA sequence. After the final synthesis cycle was completed, the resin was washed with NMP (×5), DCM (×6), and then dried.

4.2 Synthesis of 5-amino-2,9-dimethyl-1,10-phenanthroline and phenyl (2,9-dimethyl-1,10-phenanthrolin-5-yl)carbamate

5-amino-2,9-dimethyl-1,10-phenanthroline (compound **3**) was synthesised by Merita Murtola and by Partha Pratim Bose according to previously published procedures (see scheme 1).[106,114] Phenyl (2,9-dimethyl-1,10-phenanthrolin-5-yl)carbamate (compound **4**) was synthesised from compound **3** by the author of this thesis and by Partha Pratim Bose following the literature procedure shown in scheme 1.[106]

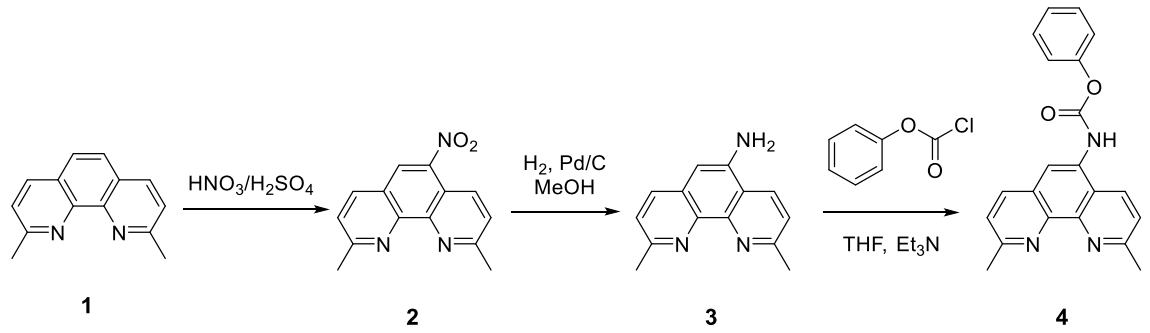

Scheme 1. Synthetic route from neocuproine **1** to 5-amino-2,9-dimethyl-1,10-phenanthroline **3** and the corresponding phenyl carbamate **4** as published previously[106]

4.3 Synthesis of 3,6-dimethyl-dipyridophenazine-11-carboxylic acid

3,6-dimethyl-dipyrido[3,2-a:2′,3′-c]phenazine)-11-carboxylic acid (referred to as dimethyl-dppz-COOH, compound **6**) was synthesised by Peter Steunenberg and Partha Pratim Bose according to the following procedure (see scheme 2), described in paper II.

Neocuproine (2.08 g, 10 mmol) (compound **1**) and potassium bromide (6.5 g, 55 mmol) were cooled on dry ice. Sulfuric acid (Conc., 98%, 44 ml) was added dropwise, forming a yellow paste. Nitric acid (Conc., 70%, 24 mL) was added dropwise while stirring (on dry ice) and a colour change from yellow to dark orange was observed. The reaction vessel was allowed to react at room temperature for 1.5 h. After that the reaction mixture was refluxed for 16 h at 86 °C with a slow increase in temperature. After the reaction mixture reached room temperature, bromine vapor was removed by blowing a stream of air over the solution and the red solution was poured in ice-water mixture (1500 mL). The pH was monitored, and solid potassium carbonate added until the mixture attained neutral pH. The resulting yellow solution was extracted with DCM (5 × 100 ml). The combined organic layers were washed with brine (2 × 100 mL) and dried with sodium sulfate. The solvents were removed in vacuo, resulting in a pale-yellow solid, 2,9-dimethyl-1,10-phenanthroline-5,6-dione (2.1g; 88%) (compound **5**).[115]

^{1}H NMR (300 MHz, CDCl3): δ (ppm) 8.41 (2H, d, ^{3}JH–H = 7.97 Hz), 7.45 (2H, d, ^{3}JH–H = 7:97 Hz), 2.88 (6H, s).

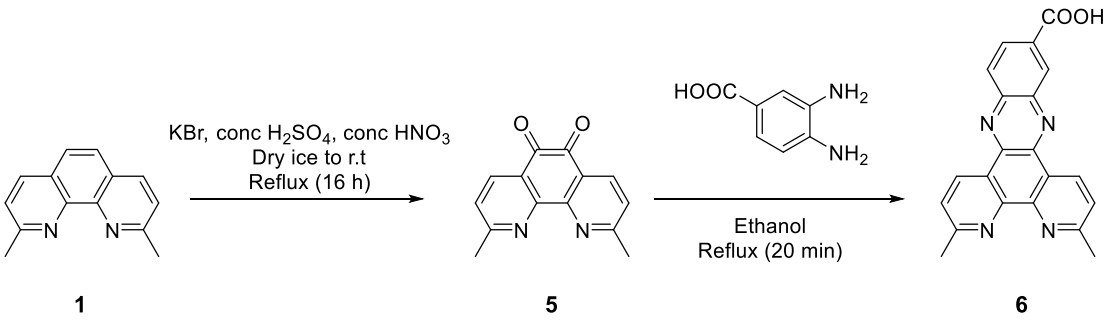

Scheme 2. Synthesis of dimethyl-dppz-COOH from dimethyl-phenanthroline (neocuproine)

2,9-Dimethyl-1,10-phenanthroline-5,6-dione (1.9 g, 8 mmol) (Compound **5**) was dissolved in ethanol (160 ml) while the temperature was increased to 50 °C under stirring for 15 min. Then, 3,4-diamino benzoic acid (1.22 g, 8.0 mmol) was added and the mixture heated under reflux for 20 min while stirring. As the reaction mixture was allowed to cool to room temperature, the product precipitated out and was filtered and washed with methanol to give a yellowish orange powder, 3,6-dimethyl-dipyrido[3,2-a:2′,3′-c]phenazine)-11-carboxylic acid (2.1 g; 75%) (compound **6**).

^{1}H NMR (300 MHz, $CDCl_3$ with a drop of TFA): δ (ppm) 10.06 -10.04 (2H, d), 9.31 (1H, S), 8.67-8.60 (2H, m), 8.21-8.19 (2H, d), 3.13-3.12 (6H, d). **ESI-TOF ES$^+$** $[M+H]^+$ calculated 355, observed 355.

4.4 Preparation of PNA conjugates

Post-synthetic conjugation reactions of the "molecular scissors" to the PNA sequences were carried out on the resin. As per previously published protocols (scheme 3),[113] the resin-bound PNA (6.4 mg, approx. 0.89 µmol) was subjected to 1% trifluoroacetic acid (TFA) in dichloromethane (DCM) for 5 × 1 min to orthogonally remove the methyltrityl (Mtt) protecting group of 2,3-diaminopropionic acid. The resin was then washed with DCM, NMP, 1% NMM in NMP and NMP. Post-conjugation was then performed according to the following procedures.

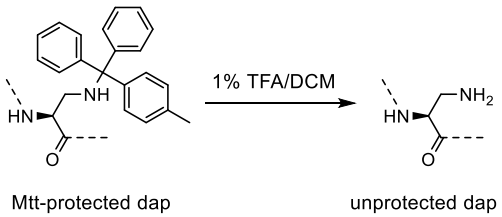

Scheme 3. Deprotection of Mtt-protected diaminopropionic acid (dap) to allow for the attachment of the chelating moieties

PNA-dimethyl-phenanthroline (neocuproine) conjugates were prepared according to previously published methods detailed below.[87,113]

Method 1: PNA-neocuproine conjugation in paper I was performed by Merita Murtola according to the previously reported method 1 as follows.[87] 5-amino-2,9-dimethyl-1,10-

phenanthroline (compound **3**) (10 mg, 45 µmol) was dissolved in DCM (200 µL). 4-methylmorpholine (NMM, 10 µL, 90 µmol) and phenyl chloroformate (5 µL, 40 µmol) were added to the solution, and the reaction mixture was agitated for 1 h. The mixture was partitioned between DCM and H_2O (200 µL). The organic phase was added to the resin-bound PNA along with a further portion of NMM (50 µL). The mixture was allowed to react overnight at room temperature. The mixture was then filtered, and the resin washed with NMP and DCM. The PNA-phenanthrene conjugate in paper I was also prepared by Merita Murtola according to method 1, except 9-aminophenanthrene was used instead of 5-amino-2,9-dimethyl-1,10-phenanthroline.

Method 2: PNA-neocuproine conjugation in papers I and II was performed according to the previously reported method 2 (scheme 4) as follows.[113] Phenyl (2,9-dimethyl-1,10-phenanthrolin-5-yl)carbamate (compound **4**) (5 µmol), NMM (20 µmol) and NMP (17 µL) were added to the resin-bound PNA. The reaction was allowed to proceed overnight at room temperature. The mixture was then filtered, and the resin washed with NMP and DCM.

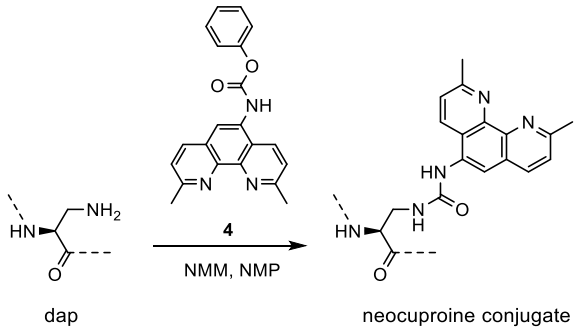

Scheme 4. Neocuproine conjugation to diaminopropionic acid

PNA-dimethyl-dipyridophenazine conjugates in papers II and III were prepared according to the following procedure (scheme 5). Prior to post-conjugation, the resin was allowed to swell in DMSO (40 uL) at 70 °C (microwave heating) over a period of 20 min. Dimethyl-dppz-COOH (2.86 mg, 8 µmol) (compound **6**) was dissolved in 110 µL of 10% NMM in 1,2-dichlorobenzene/DMSO (1:1 v/v) by extended sonication while heating at 55-60 °C. The amide coupling agent HATU (2.85 mg, 7.5 µmol in 10 µL dry DMSO) was added and the mixture agitated over a period of 7 min to allow for pre-activation of the carboxylic acid. The preactivated mixture was then added to the resin along with a further portion of NMM (30 µL) and the mixture subjected to microwave heating (75 °C) for 3 × 6 min. The resin was then washed with 1,2-dichlorobenzene, DMSO, NMP, DCM, and dried.

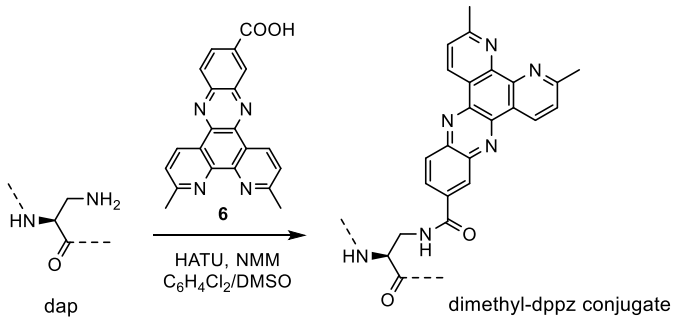

Scheme 5. Dimethyl-dipyridophenazine conjugation to diaminopropionic acid

The PNA conjugates were cleaved from the resin by treatment with the cleavage cocktail TFA-H_2O-TIS (95: 2.5: 2.5, *v/v/v*) for 1.5 h at room temperature.[112] This was followed by filtration and evaporation to dryness under a flow of N_2. The conjugates were then dissolved in water. The dimethyl-dppz conjugates were evaporated to dryness under reduced pressure. The neocuproine and phenanthrene conjugates were partitioned between water and diethyl ether, and the water layer evaporated to dryness under reduced pressure. The crude conjugates were redissolved in water and purified by RP-HPLC.

RP-HPLC analysis and purification was carried out on a Jasco HPLC system, using an Ascentis Express Supelco Peptide ES-C18 column (2.7 μm, 150 × 4.6 mm) with an eluent system of (A) milli-Q water containing 0.1% TFA, and (B) 50% MeCN: milli-Q water containing 0.1% TFA. Linear gradient elution of 0-40% B over 30 min was used at a flow rate of 1.0 mL/min at 60 °C with UV detection at 260 nm. Collected products were evaporated to dryness and lyophilised from water (×3).

The purified PNA conjugates were analysed on a Bruker Ultraflex MALDI-TOF mass spectrometer in positive ion mode using a sinapic acid matrix (10 mg/mL sinapic acid in acetonitrile-water (1:1, *v/v*) containing 0.1% TFA).[116] The MALDI-TOF MS observed m/z values are quoted in the experimental sections of papers I, II and III.

Concentrations of PNA conjugates were determined by UV absorption at 260 nm on a Varian Cary 300 UV-Vis dual beam spectrophotometer and calculated from extinction coefficients obtained by the nearest neighbour approximation,[111] and the reported extinction coefficients for phenanthroline[117] and dipyridophenazine.[118]

4.5 RNA cleavage experiments

The detailed experimental procedures for the RNA cleavage experiments have been published previously,[88,89] as well as in papers I, II and III. Some of the RNA cleavage experiments in paper I were performed by Merita Murtola and Alice Ghidini.

RNA cleavage experiments were performed in nuclease-free water for molecular biology in sealed tubes immersed in a thermostated water bath (37 °C). Low-retention pipette tips were used to transfer PNA. The protocols for RNA cleavage experiments varied between Cu^{2+} (paper I) and Zn^{2+}-dependent (papers II and III) cleavage experiments. RNA oligomers (4 μM

final concentration) were added to appropriate amounts of water and HEPES buffer (10 mM HEPES, 0.1 M NaCl final concentration, pH 7.0 or as specified). In Zn^{2+}-dependent cleavage experiments, due to the relatively weaker binding of Zn^{2+} ions by the chelating moieties, EDTA (10 μM final concentration) was added to mitigate any potential metal contamination that would render the chelate inactive. The reaction mixtures were then allowed to equilibrate over a 15-minute period at 37 °C. The metal cofactor was then added, either $Cu(NO_3)_2$ (*aq*) (10 μM final concentration) or $Zn(NO_3)_2$ (*aq*) (110 μM which leads to 100 μM effective final concentration of accessible zinc ions in the presence of 10 μM EDTA) Finally, the PNA conjugate was added (1.0-1.4 equivalents as specified) (t = 0). The reaction mixtures were then allowed to incubate at 37 °C until quenched at specified time points with an EDTA solution (2000 μM EDTA in 30% MeCN/*aq*).

The experimental procedure above was modified in turnover experiments, where an excess of RNA was required. Turnover experiments in paper I were performed with a 10-fold excess of the RNA target, which was achieved using 4 μM RNA and 0.4 μM PNA conjugate. The metal cofactor concentration remained unchanged at 10 μM Cu^{2+}. Turnover experiments in papers II and III were performed with a 33-fold excess of the RNA target, using 100 μM RNA and 3 μM PNA conjugate. The metal cofactor concentration remained unchanged at 100 μM accessible Zn^{2+} ions.

The quenched samples were analysed by anion exchange HPLC (IEX-HPLC) on a Jasco HPLC system using a Dionex NucleoPac PA-100 (4 × 250 mm) column with an eluent system of (A) 20 mM NaOAc in 30% MeCN/*aq*, and (B) 20 mM NaOAc, 0.4 M $LiClO_4$ in 30% MeCN/*aq*. Linear gradient elution of 0–45% buffer B over 30 min was used at 60 °C at a flow rate of 1.5 mL/min with UV detection at 260 nm. The extent of cleavage of RNA substrates was based on the quantification of the remaining intact RNA target and the sum of the formed RNA fragments detected at 260 nm. Representative chromatograms are provided in the Supplementary Information of papers I, II and III. The % RNA cleavage values presented are average values of at least two experiments with a standard deviation of less than ± 5% unless specified otherwise.

4.6 Determination of RNA cleavage sites

In paper I, the RNA cleavage fragments were identified by Merita Murtola. The fragments were isolated from quenched reaction aliquots by IEX-HPLC using the method detailed above and desalted by ion pairing HPLC using Supelco Discovery BIO Wide Pore C18-5.5 μm (250 × 4.6 mm, 5 μm particle size, 300 Å pore size) column and an eluent system of (A) 50 mM triethylammonium acetate (TEAA) in water (pH 6.5) and (B) 50 mM TEAA in water (pH 6.5)-acetonitrile (1:1, *v/v*). A linear gradient of 0–37 % buffer B over 20 min was used at a flow rate of 1 mL/min at 50 °C. The collected RNA fragments were then lyophilised and identified by ES mass spectrometry in negative ion mode using a solution of MeCN–water (1:1, v/v). The MS spectra are available in the Supplementary Information of paper I.

In paper II, the reaction aliquots were quenched after a 2-hour incubation period and the RNA fragments isolated by ion-pairing reversed phase HPLC as described above for paper I, except with a linear gradient of 0-20% buffer B in 20 min. The cleaved RNA fragments were collected and lyophilised. The RNA fragments were then dissolved in water and analysed by Rouven Stulz as follows. HRMS spectra were collected by elution of the oligonucleotide on a XBridge C18 column using a 0.3 ml/min linear gradient from 20 to 70% acetonitrile in 10 mM tributylammonium acetate over 8 min at 60 °C on Waters BioAccord system with a TOF mass analyser. Ionization mode: ESI negative. Source capillary voltage: 800 V. Source desolvation temperature: 550 °C. Full scan with fragmentation, mass range: 400–5000 and 2 Hz scan rate. The observed HRMS m/z values are shown in the Supplementary Information of paper II.

In paper III, the reaction aliquots were quenched after a 22-hour incubation period. The aliquots were then analysed by Kristina Karalė as follows. The samples were analysed on an Oligonucleotide BEH C18 (2.1 x 50mm, 130 Å, 3µm) column using a 0.4 ml/min linear gradient from 0 to 80% acetonitrile in 8.6 mM TEA + 100 mM HFIP buffer over 15 min at 40 °C on Waters Xevo G2-XS QTof. Ionization mode: ESI negative. Source capillary voltage: 2 kV. Source desolvation temperature: 320 °C. Full scan with fragmentation, mass range: 400-2000 Da /0.5 sec, sensitivity mode. Deconvoluted using 5 ppm tolerance. The observed monoisotopic masses and spectra are shown in the Supplementary Information of paper III.

4.7 Thermal melting analysis

As presented in paper II, UV melting experiments were performed at 260 nm on a Varian Cary 300 UV/VIS dual beam spectrophotometer (Varian). Samples containing RNA and PNA, each at a concentration of 4 µM, were analysed in 10 mM phosphate buffer containing 100 mM NaCl and 0.1 mM EDTA at pH 7.0. Initially, the temperature was rapidly increased (5 °C/min) from 20 to 90 °C and the samples heated at 90 °C for 5 min. The temperature was then decreased (3 °C/min) back to 20 °C and the samples equilibrated for 10 min. Melting points were then determined by slowly increasing (0.2 °C/min) the temperature from 20 to 90 °C and the midtransition point was calculated to yield the melting temperature (Tm) shown in the Supplementary Information of paper II.

4.8 Circular Dichroism (CD) spectroscopy

In papers II and III, CD spectra of RNA/PNAzyme complexes were measured between 230 and 370 nm on a Jasco J-1500 CD Spectrometer using 10 mm path length cuvettes. The spectra were recorded as an average of five scans at 25 °C and normalised by subtracting the background buffer scans. The samples of RNA/PNAzyme complexes (4 µM) were analysed in the absence of Zn^{2+} ions in 10 mM phosphate buffer containing 100 mM NaCl and 0.1 mM EDTA at pH 7.0. The spectra were smoothed over 5 points. The data are shown in the Supplementary Information of papers II and III.

4.9 Ethical Considerations

The research presented in this thesis was limited to chemical synthesis and analysis and thus ethical permits were not required.

5 RESULTS AND DISCUSSION

5.1 Further probing of Cu^{2+}-dependent PNAzymes (Paper I)

Cu^{2+}-dependent PNA-neocuproine conjugates have been previously shown to cleave 4-nucleotide AUAA bulge-forming RNA targets site-specifically with half-lives of around 30 minutes or less.[88,89] In paper I of this thesis, the activity of these Cu^{2+} PNAzymes was investigated further to gain a deeper understanding of the influence of bulge length and composition and the length of the RNA/PNAzyme complex on the RNA cleavage activity.

5.1.1 Cleavage of 3-nucleotide bulge-forming RNA targets

In paper I, RNA targets 1-15 (Table 1, the numbering of RNA sequences in section 5.1 is identical to the numbering in paper I) forming 3-nucleotide bulges upon binding of the PNAzyme I were shown to be cleaved by the Cu^{2+}-neocuproine PNAzyme, although at a significantly lower rate than their 4-nucleotide counterparts in previous reports.[88,89] Expectedly, the RNA cleavage rate was strongly dependent on the RNA bulge sequence.

Table 1. Schematic representation of complexes between 3-nucleotide bulge-forming RNA targets **1-15** and Cu^{2+} neocuproine PNAzymes, followed by the extent of RNA cleavage observed after incubation in the presence of 10 µM Cu^{2+} at pH 7.4 over a period of 3 h and 24 h. This table is reproduced from Luige *et al*, *Molecules* 2019, ***24***(4), 672 (paper I).

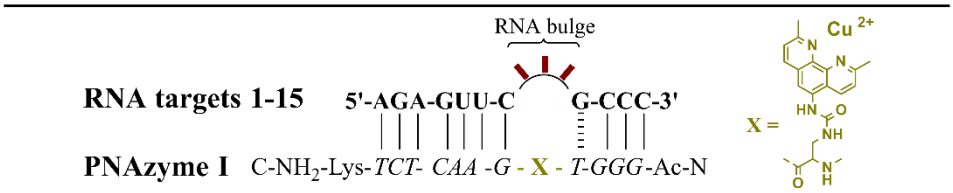

RNA	RNA bulge sequence	% RNA cleaved	
		3 h	24 h
1	**-AAA-**	18	56
2	**-AUA-**	6	19
3	**-AGA-**	14	49
4	**-ACA-**	3	11
5	**-AAU-**	<2	3
6	**-UAA-**	19	69
7	**-AUG-**	<2	6
8	**-AUC-**	<2	<2
9	**-AUU-**	<2	2
10	**-GUA-**	3	13
11	**-CUA-**	4	19
12	**-UUA-**	6	28
13	**-GUG-**	<2	5
14	**-CUC-**	<2	3
15	**-ACG-**	<2	4

Interestingly, the bulge sequence preferences observed for 3-nucleotide bulges were shown to bear keen resemblance to those previously reported for 4-nucleotide bulges.[89] The preferred RNA bulges in the respective systems were of the sequences UAA and AUAA, while the exclusion of the first adenosine nucleotide resulted in a kinetic penalty, increasing the estimated RNA cleavage half-life from 30 min to approximately 14 h. The significant disadvantage in the system where the RNA forms a 3-nucleotide bulge suggests that the structural arrangement in the bulge is profoundly affected. Generally, bulged out nucleotides in nucleic acid double strands can adopt diverse conformations, which are affected by the competing interactions of the unpaired nucleotides as well as the surrounding base pairs.[119] For example, prior molecular dynamics simulations of 4-nucleotide AAAA bulges closed with a GU wobble on the 3' side, similarly to the system at hand, have indicated that the first bulge adenosine on the 5' side participates in cross-strand stacking interactions.[120] The precise structure of the bulge in the RNA/PNAzyme I complexes cannot be elucidated at this point, but evidently, the interactions of the first bulge adenosine in the RNA/PNAzyme complex are significant, and their elimination critically impacts the structure of the RNA bulge in the vicinity of cleavage site.

5.1.2 Modified 4-nucleotide bulge-forming RNA targets

The A/A cleavage site in the fastest cleaved 4-nucleotide AUAA bulge was then probed by introducing critical chemical modifications into the structure of the central adenosine nucleotide (Table 2). Both the exocyclic amino group and the 2'-hydroxyl group of the adenosine (AU**A***A) were shown to be critical for PNAzyme I-promoted RNA cleavage. The exocyclic amine was thus suggested to have a critical role in coordinating the Cu^{2+} ion. The 2'-hydroxyl group was also shown to be critical, which was expected due to its role as the nucleophile in the transesterification reaction leading to RNA cleavage.

Table 2. Schematic representation of RNA/PNAzyme complexes where the 4-nucleotide AUAA bulge-forming RNA targets contained critical chemical modifications in the central adenosine A*, or the PNA-neocuproine (X) conjugate was replaced with a PNA-phenanthrene (Y) conjugate, followed by the extent of RNA cleavage after incubation of these complexes in the presence of 10 µM Cu^{2+} at pH 7 over a period of 1 h, 3 h and 24 h. This table is reproduced from Luige *et al*, *Molecules* 2019, ***24***(4), 672 (paper I).

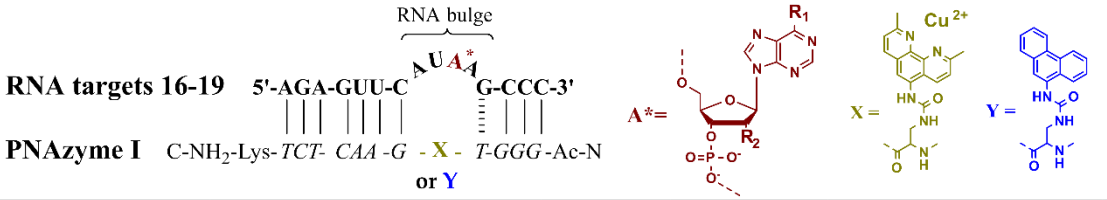

RNA	Conjugate	Bulge modification (A*)	R_1	R_2	% RNA cleaved		
					1 h	3 h	24 h
16	**X**	Unmodified adenosine	NH_2	OH	71		
17	**X**	Purine	H	OH		15	46
18	**X**	Deoxyadenosine	NH_2	H		1	5
19	**X**	2′-O-Methyladenosine	NH_2	OMe		3	7
16	**Y**	Unmodified adenosine	NH_2	OH		n.d.	n.d.

Moreover, it has been previously suggested that activation of phosphodiesters by "pin-point" activation could be achieved when nucleobases interact with polyaromatic molecules.[121,122] In other words, interactions between the polyaromatic "molecular scissors"-like moieties could activate phosphodiesters, thus facilitating RNA cleavage in the presence of external metal ions. If such interactions were significant in PNAzyme-mediated RNA cleavage, then activity should be observed also with the equivalent PNA-phenanthrene conjugate (Table 2, Y) in the presence of free Cu^{2+} ions in solution. The PNA-phenanthrene conjugate was not able to promote RNA cleavage, demonstrating that the PNAzyme's ability to chelate a metal ion is critical.

5.1.3 Elongation of the PNAzyme sequence

The influence of elongation of the RNA/PNAzyme complex was another aspect of interest. The short recognition arm of the RNA/PNAzyme complex consists of a GT wobble base pair closing the bulge, followed by three CG base pairs. The weak GT wobble base pair has been shown to be critical in previous studies, as a GC Watson-Crick base pair in this position leads to significant loss of activity.[89] It could be hypothesised that the sequence of the short recognition arm is significant for the PNAzymes activity, for example, if partial unwinding or "breathing" of the double helix occurs. Such occurrence could, however, be prevented by extending this recognition arm by additional Watson-Crick base pairs, thus increasing its stability. On the other hand, if elongation of the complex is tolerated, then the increased stability could be useful, *e.g.* for further studies such as structure determination by x-ray crystallography.

Table 3. Schematic representation of complexes between PNAzymes I and II and 4-nucleotide bulge-forming RNA targets, where the PNAzyme extension leads to a PNA overhang, followed by the extent of RNA cleavage after incubation in the presence of equimolar PNAzyme I or II and 10 µM Cu^{2+} at pH 7 over a period of 30 min. This table is reproduced from Luige *et al*, *Molecules* 2019, ***24***(4), 672 (paper I).

RNA 20-22/ ***PNAzyme*** **I**

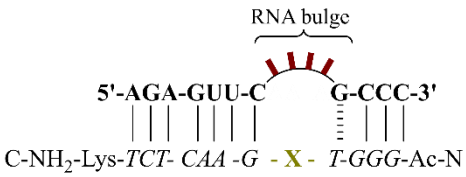

RNA 20-22/ ***PNAzyme*** **II**

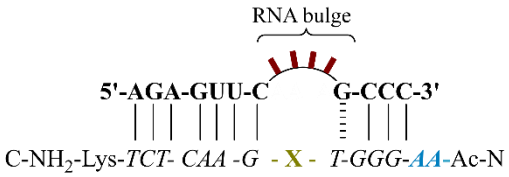

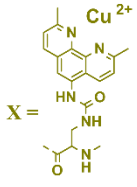

RNA	Bulge sequence	% RNA cleaved after 30 min	
		PNAzyme I	PNAzyme II
16	**-AUAA-**	**58**	40
20	**-AAUA-**	2	< 2
21	**-AAAA-**	36	23
22	**-ACAA-**	54	45

An elongated PNAzyme II was synthesised, where the sequence was extended by 2 nucleobases (Table 3). Initially, the extended PNAzyme was studied in conjunction with the previously studied[89] 4-nucleotide bulge-forming RNA target sequences (Table 3, RNAs 16, 20-22), thus forming a short PNAzyme overhang. Interestingly, the RNA cleavage activity was slightly decreased in the presence of the PNA overhang, compared to the activity of PNAzyme I lacking the overhang. These findings are yet another example of the sensitivity and specificity of PNAzyme action. In addition to excellent mismatch discrimination demonstrated in earlier work,[89] the PNAzyme would be expected to exhibit lower cleavage activity in case of binding to a potential off-target RNA sequence where the recognition arm is incomplete.

Elongation of the entire complex in the short recognition arm leads to increased binding strength, thus inhibiting any partial unwinding or "breathing" of the helix. Whether such unwinding occurs, or if so, then how it affects the PNAzyme activity was a key question in this study. A longer and more complex RNA target sequence (Fig 10, RNA 23) was investigated, where the PNAzyme could bind to the RNA target in a region containing a complete set of recognition arms (Fig 10, Scenario 1), or in a competing region where the short recognition arm contained a mismatch (Fig 10, Scenario 2).

The elongated PNAzyme II forms two additional Watson-Crick base pairs with RNA 23 when bound to the preferred binding region, thus extending the short recognition arm. Elongation of the short recognition arm from 3 Watson-Crick base pairs and a wobble to 5 Watson-Crick base pairs and a wobble did not affect the cleavage rate, as the longer target RNA 23 was cleaved by the elongated PNAzyme II to the same extent as RNA 16 by the short PNAzyme I (Table 4). It has been previously shown that the mismatch in the short recognition arm depicted in Fig 10 Scenario 2 renders the system catalytically inactive and cleavage fragments corresponding to this binding scenario are not observed.[89]

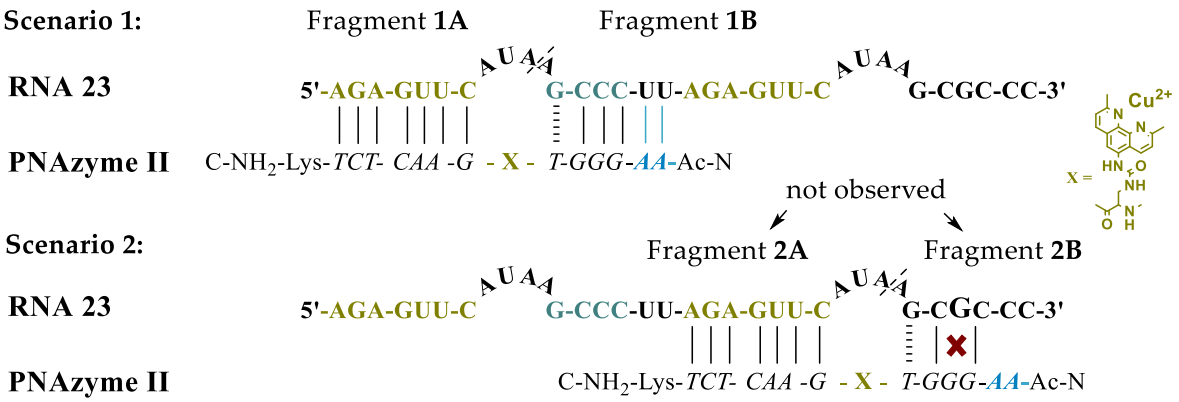

Figure 10. Possible complexes between RNA 23 and PNAzyme II. The dashed line denotes the cleavage site. This figure is reproduced from Luige *et al*, *Molecules* 2019, ***24***(4), 672 (paper I).

Table 4. The extent of cleavage of RNAs **23** and **24** after incubation in the presence of PNAzyme **I** or **II** and 10 μM Cu^{2+} at pH 7 over a period of 30 min and 1 h. This table is reproduced from Luige *et al*, *Molecules* 2019, ***24***(4), 672 (paper I).

RNA	PNAzyme	% RNA cleaved	
		30 min	1 h
23	**I**	37	55
	II	59	79
24	**II**	37	54

Rather interestingly, however, the short PNAzyme I was not able to cleave the long RNA 23 as efficiently. The reason for the decrease in the cleavage rate could have been a greater degree of binding to the competing recognition arms (Fig 10, Scenario 2). Elongation of the recognition arms increases the binding strength and thus shifts the equilibrium further towards binding to the complete recognition arms. As such, elongation of the PNAzyme was necessary to retain the fast cleavage rate on this elongated more complex RNA target. Moreover, despite the increase in the binding strength that could theoretically inhibit dissociation of the cleaved fragments, the elongated PNAzyme was able to turn over multiple RNA 23 substrate molecules in turnover experiments with a 10-fold excess of the RNA target over 24 h.

In contrast, a decrease was observed in the rate of cleavage of another elongated RNA target (RNA 24, Fig 11) by PNAzyme II where the alternative binding region was able to offer more competition due to the lack of a mismatch (Scenario 2, Fig 11). PNAzyme binding to the competing region resulted in the formation of an essentially uncleavable bulge,[89] but this alternative scenario was clearly able to sequester more of the PNAzyme, thus hindering its ability to bind the preferred binding region which ultimately results in slower cleavage (Table 4). Moreover, this decrease in activity could have been further compounded by the single nucleotide overhang (Scenario 1, Fig 11).

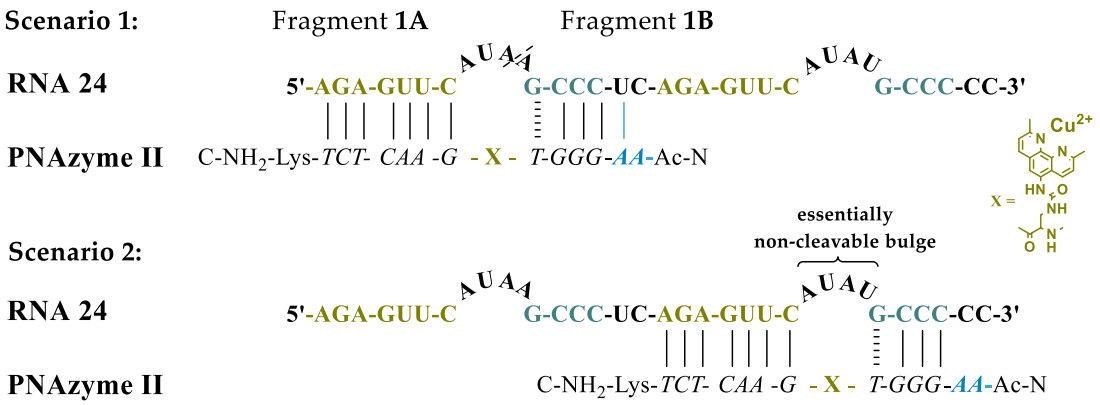

Figure 11. Possible complexes between RNA 24 and PNAzyme II. The dashed line denotes the cleavage site. This figure is reproduced from Luige *et al*, *Molecules* 2019, ***24***(4), 672 (paper I).

5.2 Zn^{2+}-dimethyl-dppz-PNA conjugates as artificial ribonucleases (Paper II)

Metal cofactor-dependent artificial ribonucleases require a sufficient local concentration of the cofactor in the cellular environment to maintain their RNA cleavage activity. However, free copper is rarely available in cells,[110] and therefore Cu^{2+}-dependent PNAzymes are less feasible in therapeutic contexts. On the other hand, Zn^{2+} is an important metal for cellular processes and present at various concentrations in cells.[123] As such, Zn^{2+} ion-dependent PNAzymes have greater potential for therapeutic purposes. However, the RNA cleavage rates of Zn^{2+}-dependent artificial ribonucleases[87,104–107] have been far inferior to their Cu^{2+}-dependent counterparts. In paper II, dimethyl-dipyridophenazine (dppz) was investigated as "molecular scissors" conjugated to PNA for the potential of PNA-dimethyl-dppz conjugates to act as efficient Zn^{2+}-dependent PNAzymes that cleave RNA bulges.

Dimethyl-dipyridophenazine is a heterocyclic aromatic compound and an extended phenanthroline derivative (Fig 12) that has been widely utilised in applications involving nucleic acids as an intercalator. Intercalation occurs when large rigid hydrophobic heterocycles insert themselves and stack between nucleobases.[124] Intercalative binding between nucleic acids and dipyridophenazine has been used in numerous applications,[125] including the octahedral $[Ru(bpy)_2(dppz)]^{2+}$ complex that acts as a molecular "light switch" detecting DNA[126], a luminescent probe for the detection of RNA mismatches,[127] and dppz-based Zn(II) complexes as DNA photocleavers[128] among others.

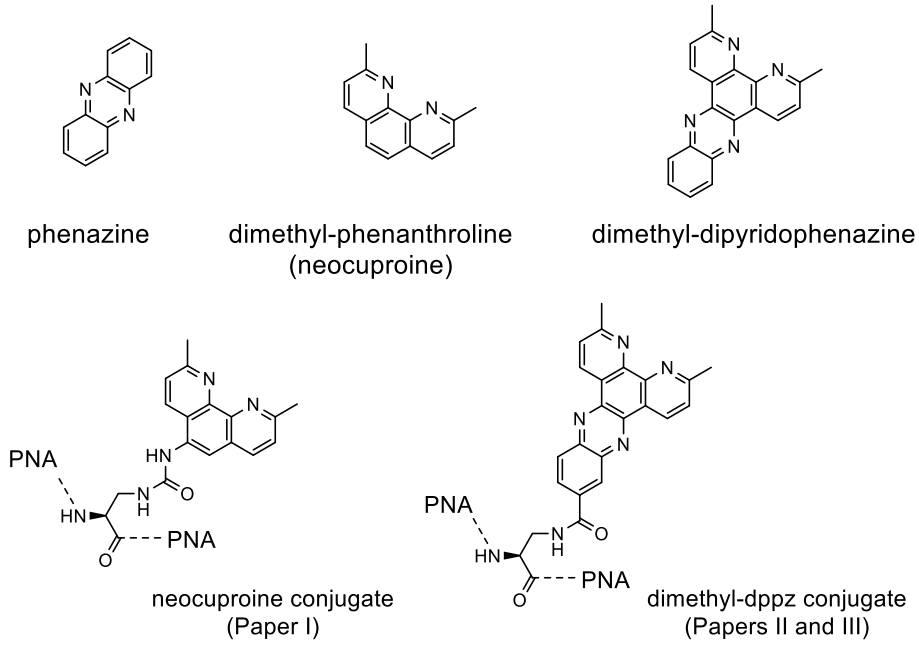

Figure 12. Structures of phenazine, dimethyl-phenanthroline and dimethyl-dppz.

In paper II, dimethyl-dppz-carboxylic acid (compound **6** in section 4.3) was synthesised and conjugated to PNA to create novel PNAzymes (Fig 12). The cleavage activity of the resulting dimethyl-dppz-PNA conjugates was then investigated on various RNA targets (note that in the interest of clarity, the numbering of RNA target sequences and PNAzymes in section 5.2 is identical to the numbering in paper II, but therefore different from 5.1 and paper I).

5.2.1 RNA cleavage by Zn^{2+}-dimethyl-dppz PNAzymes

The initial RNA target (RNA 1 in paper II) was a leukaemia-related bcr/abl mRNA model previously studied in conjunction with Cu^{2+} and Zn^{2+} neocuproine PNAzymes.[87,89] The 4-nucleotide AAAA bulge-forming RNA target (Fig 13a) was cleaved by the Zn^{2+}-dependent dimethyl-dppz PNAzyme (PNAzyme I in paper II) with an approximately 3 h half-life at pH 7.0 at 37 °C in the presence of Zn^{2+} ions (100 µM). RNA fragments originating from two nearly equally favoured cleavage sites were detected (Fig 13c). Furthermore, targeting an RNA sequence designed to form a smaller 3-nucleotide AAA bulge led to a significantly enhanced cleavage rate (RNA 2, Fig 13b). The cleavage of RNA 2 occurred at a single site with a half-life of approximately 1 h (Fig 13d), which is significantly faster than the cleavage accomplished with Zn^{2+}-dependent neocuproine-based PNAzymes.[87]

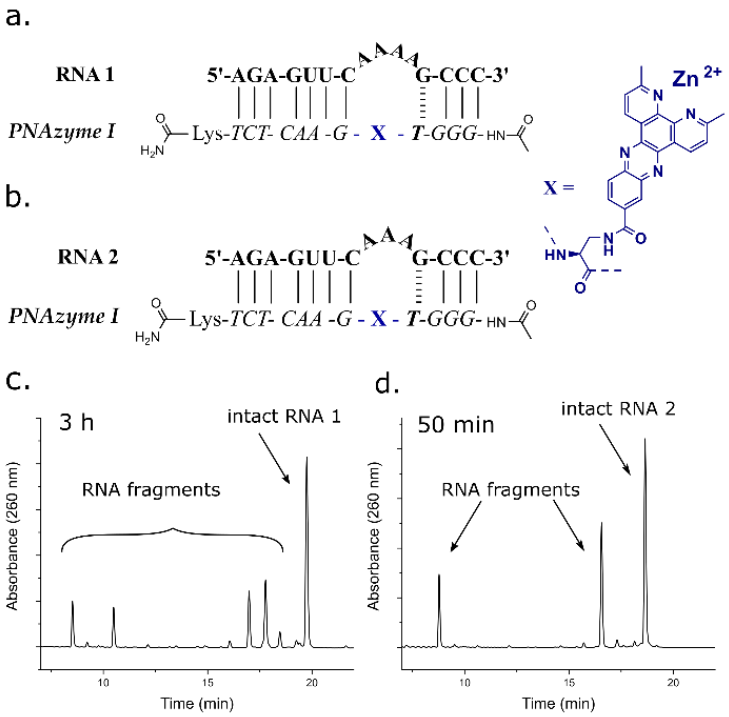

Figure 13. Schematic representations of PNAzyme I complexes with (a) RNA 1 and (b) RNA 2 where single-stranded RNA bulges of 4 or 3 adenosine nucleotides are formed. Ion-exchange HPLC chromatograms showing the extent of cleavage of (c) RNA 1 (51 ± 2% in 3 h) and (d) RNA 2 (44 ± 2% in 50 min) after incubation at 37 °C, pH 7.0 and 4 µM RNA/PNAzyme concentration in the presence of 100 µM Zn^{2+}. This figure is reproduced from Luige *et al*, *Chem. Commun*.**,** 2021, **57**, 10911-10914 (paper II).

5.2.2 Bulge sequence dependence

Further RNA target sequences that formed 3-nucleotide bulges of various sequences were then investigated (RNAs 3-16, Fig 14). The Zn^{2+} dimethyl-dppz PNAzyme-promoted cleavage of 3-nucleotide RNA bulges was shown to exhibit considerable bulge sequence-dependence. RNA bulges of the sequence UUA, AUA and GUA were cleaved with under 20-minute half-lives. Other bulge sequences were either cleaved at a lower rate or shown to be essentially uncleavable. Interestingly, the presence of adenosine in the third position in the bulge was critical to obtain any RNA cleavage within the timeframe studied. In the second

position in the bulge, uridine was clearly favoured, while all other nucleotides also led to some RNA cleavage. The first position in the bulge was able to accommodate any nucleotide, although cytidine was tolerated slightly less than the other nucleotides.

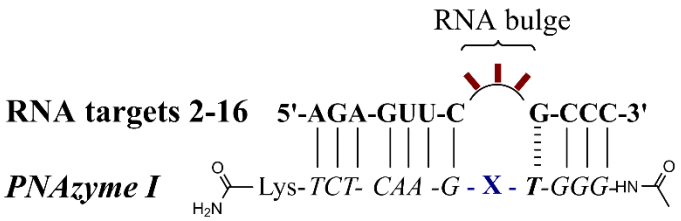

RNA	RNA bulge sequence	% RNA cleaved	
		10 min	20 min
2	**-AAA-**	11	21
3	**-AUA-**	35	58
4	**-AGA-**	18	32
5	**-ACA-**	8	15
6	**-AAU-**		n.d.
7	**-UAA-**	15	28
8	**-AUG-**		3
9	**-AUC-**		n.d.
10	**-AUU-**		n.d.
11	**-GUA-**	32	56
12	**-CUA-**	21	39
13	**-UUA-**	37	60
14	**-GUG-**		7
15	**-CUC-**		n.d.
16	**-ACG-**		n.d.

Figure 14. Schematic representation of complexes between Zn^{2+} dimethyl-dppz PNAzyme I and 3-nucleotide bulge-forming RNA targets 2-16 and the extent of RNA cleavage observed after incubation at 37 °C, pH 7.0 and 4 µM RNA/PNAzyme concentration in the presence of 100 µM Zn^{2+}. The structure of X is shown in Fig 13. This figure is adapted from Luige *et al*, *Chem. Commun.*, 2021, **57**, 10911-10914 (paper II).

Further insights were gained from the MS analysis of the cleavage fragments of the most rapidly cleaved RNA targets. The U/A internucleosidic phosphate linkage in the bulge was confirmed as the cleavage site, explaining the sensitivity to changing the sequence in this part of the bulge. The cleavage was shown to produce a 2',3'-cyclic phosphate as the longer fragment (Fig 15). Given the cleavage site, the critical adenosine nucleotide in the third position in the bulge hence has the role of providing the 5'-hydroxyl leaving group.

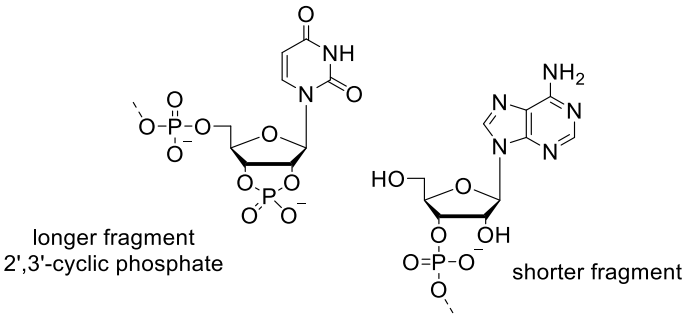

Figure 15. Structures of the 3' and 5' termini of the detected cleavage fragments – the 2',3'-cyclic phosphate as the longer fragment and the 5'-hydroxyl as the shorter fragment.

The cleavage kinetics of one of the most rapidly cleaved RNA targets (AUA bulge-forming RNA 3) was followed over 60 minutes and the resulting RNA degradation curve is depicted in Fig 16. The half-life of RNA cleavage was determined to be 16 minutes. Furthermore, The Zn^{2+} dimethyl-dppz PNAzyme's ability to give turnover of the RNA substrate was confirmed in experiments with a 33-fold excess of the RNA target with respect to the PNAzyme. After 6 hours of incubation, the PNAzyme had been able to promote the cleavage of 86 ± 4% of RNA 13 (Fig 16), demonstrating multiple turnover.

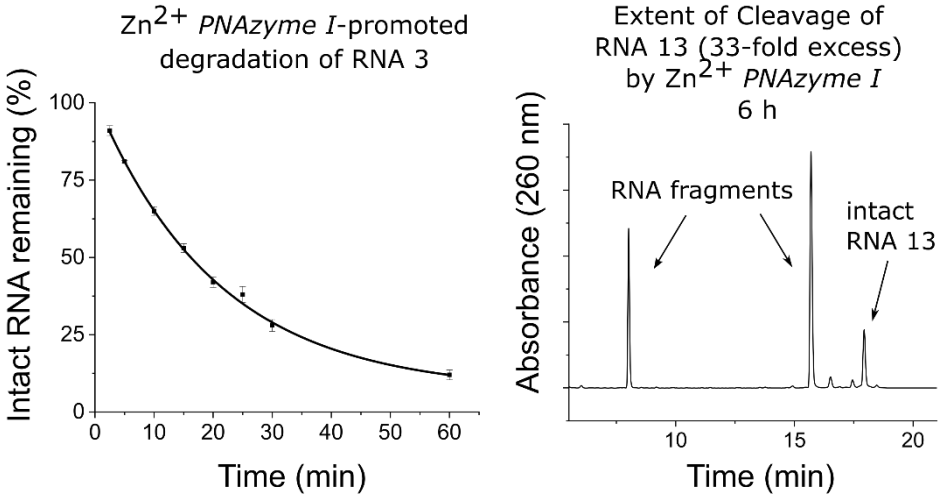

Figure 16. Left – RNA 3 (4 µM) degradation curve in the presence of Zn^{2+} ions (100 µM) and dimethyl-dppz PNAzyme I (1.4 equiv) at pH 7.0, 37 °C. Right – Representative IEX-HPLC chromatogram of turnover experiments, depicting the extent of cleavage of a 33-fold excess of RNA 13 (100 µM) after 6 h incubation in the presence of Zn^{2+} ions (100 µM) and dimethyl-dppz PNAzyme I (3 µM) at pH 7.0, 37 °C. This figure is adapted from Luige *et al*, *Chem. Commun*., 2021, 57, 10911-10914 (paper II).

As such, the cleavage activity displayed by the Zn^{2+} dimethyl-dppz PNAzyme is higher than the activity of any artificial ribonuclease reported to date, including Cu^{2+}-neocuproine PNAzymes.[88,89] In the absence of an x-ray crystal structure or more detailed structural studies, the precise role of the extended phenanthroline-based dppz "molecular scissorss" system within the PNAzyme structure is difficult to elucidate, but the enhancement of the PNAzyme activity upon the inclusion of this chelating moiety is likely to result from additional interactions that

the they have within the complex. Such interactions can potentially help to make the bulge more susceptible to cleavage due to effects on the pre-organisation of the structure. Moreover, affecting or optimising the position of the zinc ion can result in more efficient catalysis.

Circular dichroism (CD) spectroscopy as well as UV thermal melting analysis can shed some light on the structure of the RNA/PNAzyme complexes. Comparison of the CD spectra (Fig 17) of RNA 3 complexes with unconjugated PNA, PNA-neocuproine conjugate (PNAzyme I in paper I) and PNA-dimethyl-dppz conjugate (PNAzyme I in paper II) showed that the presence of the dimethyl-dppz moiety is accompanied by a significant spectral change, suggesting that the chelating moiety affects the structure of the complex. Moreover, increased interactions were also evident from the 4 °C increase in thermal melting temperature for the RNA complex with the dppz-containing conjugate compared to the complex with unconjugated PNA.

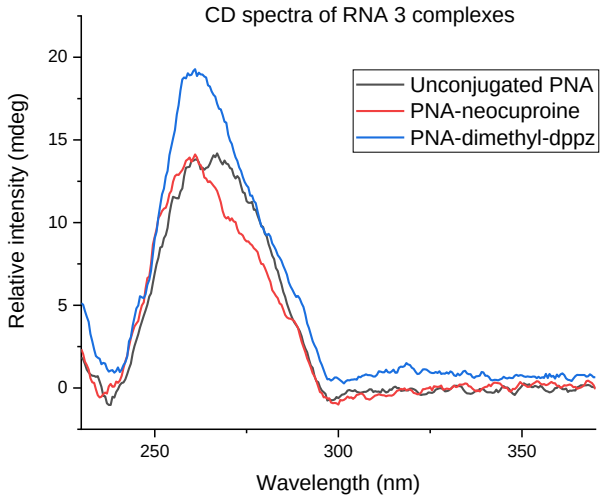

Figure 17. Circular dichroism spectra of RNA 3 complexes with unconjugated PNA and PNA conjugates. This figure is reproduced from Luige *et al*, *Chem. Commun*.**,** 2021, **57**, 10911-10914 (SI) (paper II).

In contrast to the PNA-neocuproine conjugates that cleaved RNA significantly more efficiently in the presence of Cu^{2+} rather than Zn^{2+} ions,[87,89] the PNA-dimethyl-dppz conjugate PNAzyme I cleaves just 12 ± 1% of RNA 3 in 3 hours in the presence of Cu^{2+} ions (Fig 18).

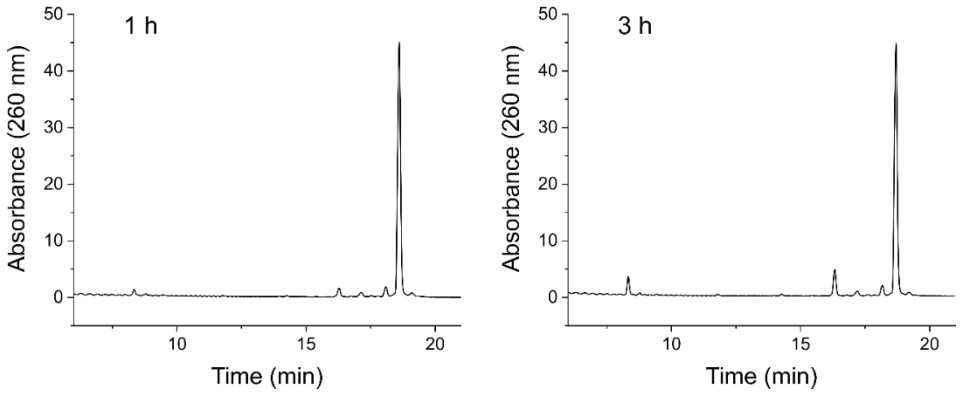

Figure 18. Dimethyl-dppz PNAzyme I-promoted cleavage of the AUA bulge-forming RNA 3 in the presence of Cu^{2+} (10 μM) in the absence of Zn^{2+} after 1 h (left) and 3 h (right) of incubation at pH 7.0, 37 °C. (Unpublished data).

5.2.3 pH dependence

The cleavage of RNA 3 was shown to depend on the pH of the buffer, displaying a bell-shaped pH-rate profile (Fig 19a). The fastest rate was observed at pH 7.4, where the cleavage half-life was approximately 10 minutes. In prior work, the fastest Zn^{2+}-dependent artificial ribonuclease activity has been achieved with Zn^{2+}-neocuproine PNAzymes, where the fastest RNA cleavage half-lives have been in the range of 7-8 hours at pH 7.4.[87] As such, the 10-minute cleavage half-life accomplished with the Zn^{2+} dimethyl-dppz PNAzyme I herein is 40-50 times faster than the previous best with Zn^{2+}-neocuproine PNAzymes.

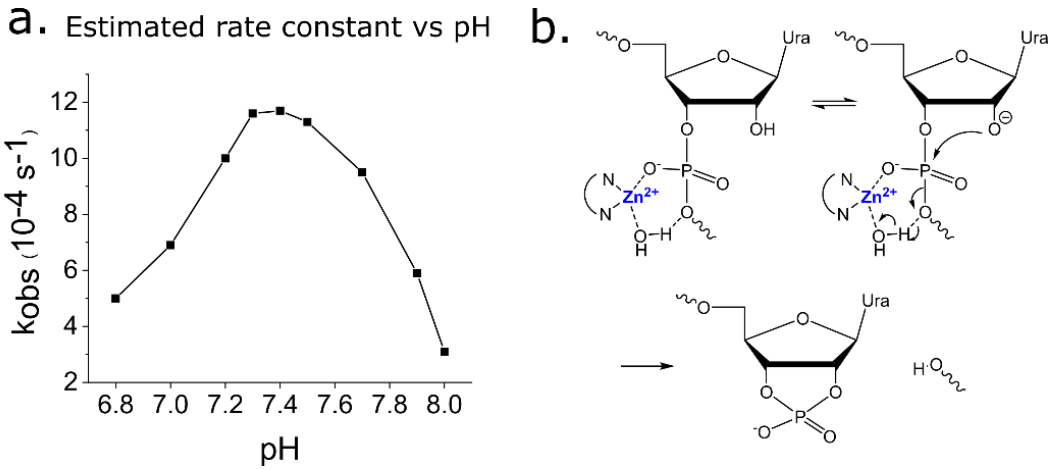

Figure 19. (a) pH-Rate profile of RNA 3 cleavage by Zn^{2+}-dimethyl-dppz PNAzyme I. (b) Hypothetical mechanism for the acid-base catalysis leading to the cleavage of RNA by Zn^{2+}-dimethyl-dppz PNAzymes. This figure is reproduced from Luige *et al*, *Chem. Commun*.**,** 2021, **57**, 10911-10914 (paper II).

The bell shape of the pH-rate profile is indicative of acid-base catalysis, involving deprotonation of the 2'-hydroxyl nucleophile and protonation of the 5'-oxygen leaving group.[129] The increase in rate between pH 6.8 and 7.4 is suggested to be due to the shifting of the equilibrium of the 2'-hydroxyl deprotonation (specific base catalysis). The decrease in the rate between pH 7.4 and 8.0 correlates with the shifting of the equilibrium of the metal-aqua complex towards the inactive metal-hydroxide that can no longer deprotonate the 5'-oxygen. As such, a hypothetical mechanism was proposed (Fig 19b), involving pre-equilibrium deprotonation and subsequent general acid catalysis by the metal aquo ion.

5.2.4 Zn^{2+} concentration dependence

In a clinical setting, another important aspect is that a sufficient local concentration of the metal cofactor is required for the PNAzymes. The Zn^{2+}-dependence study of dimethyl-dppz-PNAzyme-promoted RNA cleavage showed that approximately 100 µM Zn^{2+} ion concentration is required in order to achieve the fastest cleavage activity (Fig 20).

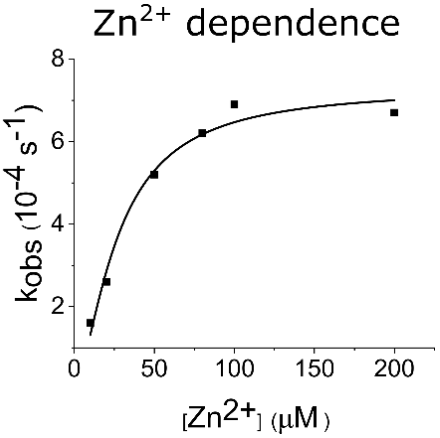

Figure 20. Estimated rate constants for the cleavage of RNA 3 by Zn^{2+}-dimethyl-dppz PNAzyme I at pH 7.0, at 37 °C at 2-200 μM Zn^{2+} concentration. The rate constants were calculated based on the cleavage data from 4 different timepoints at each zinc ion concentration, and each cleavage experiment was performed at least twice. This figure is reproduced from Luige *et al*, *Chem. Commun*.**,** 2021, **57**, 10911-10914 (SI) (paper II).

The total cellular zinc concentration in humans is reportedly 0.2-0.3 mM, but the levels of free Zn^{2+} ions are thought to be tightly controlled and maintained in the picomolar range.[123,130] Nonetheless, steep zinc gradients exist to ensure adequate zinc supply for the numerous proteins that bind zinc ions, and thus even millimolar local intracellular Zn^{2+} concentrations can be achieved.[131] Zinc ions are also found to accumulate in some tissues, for example the prostate gland[132] and the eye.[133] Furthermore, some diseases are associated with significantly elevated zinc concentrations. Extreme accumulation of zinc ions has been detected in malaria-infected red blood cells, where high levels of free Zn^{2+} are required for parasitic growth.[134] Zinc dysregulation has also been noted in Alzheimer's disease,[135] where excess zinc has been detected in the brain regions associated with memory processing and intracellular neurofibrillary tangles pathology in mice.[136] Provided that a suitable RNA target can be found, diseases associated with an increased Zn^{2+} concentration could potentially be well suited for treatment by Zn^{2+}-dependent PNAzymes.

5.2.5 Sequence considerations for the identification of novel targets and selection of clinically relevant RNA models

PNAzymes could have diverse applications in disease therapy as well as molecular biology research, but one specific example of their potential therapeutic use is inhibition of parasitic or viral infections. Finally in paper II, PNAzyme-mediated RNA cleavage of clinically relevant RNA target sequences was investigated.

The selection of novel RNA target sequences was not straightforward, as the significance of the RNA/PNAzyme sequence in the hybridised recognition arms was not known, especially in the regions near the single-stranded RNA bulge where the cleavage takes place. While the minimum requirement for an efficiently cleaved RNA target sequence could be simply the presence of one of the most rapidly cleaved bulges (UUA, AUA, GUA), a more conservative estimate was employed in paper II, aiming to find RNA target sequences that would also preserve the CG and GT bulge-closing base pairs. It was hoped that the rest of the sequence of

the RNA/PNAzyme complex will serve the role of mere sequence recognition without affecting the cleavage activity. In paper II, two clinically relevant RNA models were identified and tested. These models were based on the target sequences identified in the malaria parasite *Plasmodium falciparum* mRNA and the genomic RNA of SARS-CoV-2.

Malaria is a mosquito-borne infectious disease that continues to have a devastating impact worldwide with over 200 million cases recorded annually, leading to up to half a million deaths per year globally.[134,137] This parasitic tropical disease is predominantly caused by *Plasmodium falciparum* and this species is also responsible for the most severe malaria.[137] The devastation caused by *P. falciparum* is further compounded by its increasing drug resistance, which underscores the urgent need for new therapeutic interventions.[138] As mentioned above, it has been shown that *P. falciparum* causes an accumulation of extraordinarily high levels of zinc ions in infected red blood cells, including bioavailable free or weakly-bound Zn^{2+}, which are required in the blood-stage of the parasite life cycle.[134] Infected erythrocytes are reported to contain an average of 1 mM zinc ions, corresponding to a 4-fold increase in total zinc concentration compared to uninfected red blood cells.[139] As RNA transcription has been shown to occur early in the parasite life cycle, followed by an exponential increase in Zn^{2+} concentration in the later stages of the 48-hour cycle,[134] inhibition of protein synthesis by sequence specific degradation of parasitic mRNA by Zn^{2+}-dependent PNAzymes could potentially be a successful therapeutic strategy.

Thousands of genes in the *P. falciparum* genome have been defined as essential for parasitic growth and could therefore be considered as drug targets, including genes implicated in drug-resistance and genes with functions associated with translation, RNA metabolism and cell cycle control.[140] In fact, antisense oligonucleotides targeting mRNA have been investigated as antimalarial agents inhibiting the malarial topoisomerase II.[141,142] In paper II, a potential RNA target sequence (RNA 17, Fig 21) was identified for the Zn^{2+} PNAzymes from the *P. falciparum* exported protein 1 (EXP1) gene which encodes an integral membrane protein essential for nutrient uptake.[143,144]

Moreover, viruses pose another major global health concern, as best exemplified by severe acute respiratory syndrome coronavirus 2 (SARS-CoV-2), the virus responsible for the worldwide COVID-19 pandemic, but also other RNA viruses such as Influenza A and Dengue virus, which cause significant mortality annually.[145] Antiviral oligonucleotide therapies can be designed against DNA or RNA viruses, targeting viral RNA transcripts or viral RNA genomes.[145] The latter are particularly attractive targets for antiviral oligonucleotides, since viral RNA genome replication is the basis of infection with RNA viruses, and the RNA genomes can be directly targeted and destroyed with oligonucleotide-based therapies.[145]

The RNA genome of SARS-CoV-2 was found to contain numerous potential target sequences for the Zn^{2+}-dimethyl-dppz PNAzymes. The mRNA target sequence (RNA 18 in paper II, Fig 21) selected for this study encodes a viral protease (betacoronavirus papain-like protease, SCoV2-PLpro) which is essential for processing viral polyproteins required for a functional replicase complex which enables viral spread.[146] Moreover, inhibition of SCoV2-PLpro with a small molecule inhibitor has been shown to reduce viral replication in infected cells.[146]

Potential model target sequences were identified initially based on their compliance with the basic structural demand (the presence of the sequences 5'-C-bulge-G-3', where the bulge is AUA, UUA or GUA), and the two targets finally selected among them based on their additional similarities with the previously tested sequences (*e.g.* RNAs 3, 11, 13 in paper II).

a.

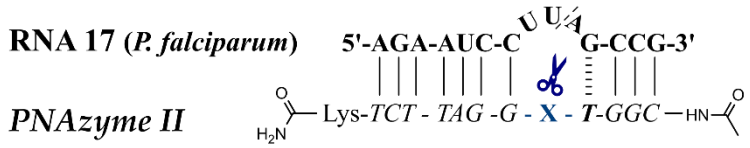

b.

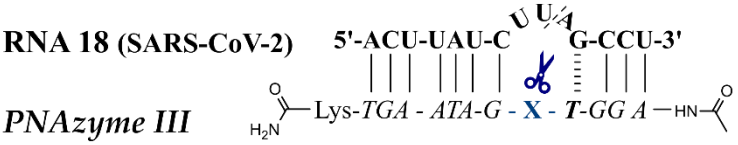

c.

RNA:PNAzyme complex	% RNA cleaved		
	5 min	10 min	20 min
RNA 17/ *PNAzyme II*	18	38	58
RNA 18/ *PNAzyme III*	17	34	54

d.

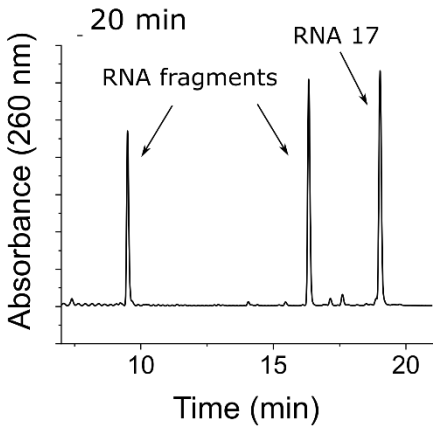

e.

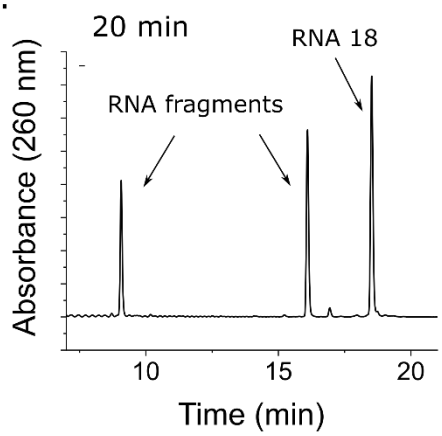

Figure 21. Schematic representations of PNAzymes II and III in complex with their respective clinically relevant RNA targets (a) a *Plasmodium falciparum* (malaria parasite) mRNA model target RNA 17 and (b) a SARS-CoV-2 genomic RNA model target RNA 18. (c) The extent of cleavage of RNA 17 and 18 by PNAzymes II and III, respectively, after 20 min of incubation. Ion-exchange HPLC chromatograms showing the extent of cleavage of (d) RNA 17 (58 ± 2%) and (e) RNA 18 (54 ± 2%) after 20 minutes of incubation at 37 °C, pH 7.0 and 4 µM RNA/PNAzyme concentration in the presence of 100 µM Zn^{2+}. The structure of X is shown in Fig 13. This figure is reproduced from Luige *et al*, *Chem. Commun.*, 2021, **57**, 10911-10914 (paper II).

The *Plasmodium falciparum* mRNA fragment (RNA 17 in paper II) as well as the SARS-CoV-2 genomic RNA fragment (RNA 18 in paper II) were cleaved efficiently by the corresponding Zn^{2+}-dimethyl-dppz PNAzymes II and III with cleavage half-lives below 20 minutes. Mass spectrometry data confirmed the UA internucleosidic linkage in the bulge as the cleavage site, as was seen for the earlier sequences above. These results are highly encouraging, as the variations in the sequence of the long recognition arm did not affect the RNA cleavage rate. As such, the Zn^{2+} PNAzymes are proving to be versatile agents that can be designed to cleave various RNA targets in a sequence and site-specific manner.

5.3 Influence of sequence variation on the RNA cleavage activity of Zn^{2+}-dependent dimethyl-dppz PNAzymes (Paper III)

Zn^{2+}-dimethyl-dppz PNAzyme-mediated cleavage of clinically relevant RNA target sequences is highly encouraging, but wider applicability of these artificial enzymes requires a thorough understanding of the sequence requirements for efficiently cleaved RNA target sequences. The goal of paper III was to understand the relationships between the sequence of the RNA/PNAzyme complex and the efficiency of RNA cleavage by Zn^{2+}-dimethyl-dppz PNAzymes, and thus to determine the extent to which the RNA target sequences can be modified while still maintaining efficient activity.

5.3.1 Sequence variation in the long recognition arm

The first line of inquiry was the bulge-closing base pair in the long recognition arm. So far, the RNA/PNAzyme complexes have contained a CG base pair as the 5' bulge-closing base pair. The cleavage of an AAA-bulge forming RNA in such a complex was shown to take place with a 1-hour half-life in paper II (see Fig 22). In paper III, four novel RNA/PNAzyme complexes were constructed (Fig 23), where the closing base pair of AAA bulges in the long recognition arm was varied (RNAs 2-5 and PNAzymes II-V in paper III, note that the numbering of RNAs and PNAzymes herein (section 5.3) is identical to the numbering in Paper III, but therefore different from 5.1 and 5.2 and papers I and II).

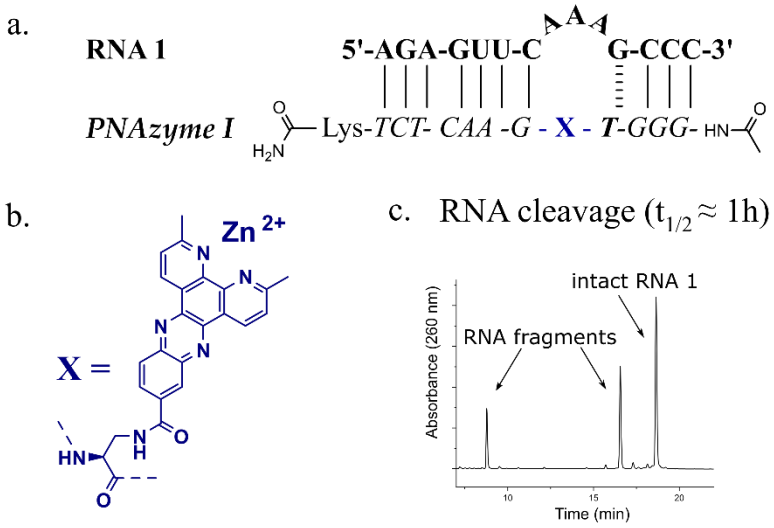

Figure 22. (a) Schematic representation of the previously reported RNA target 1 that forms a 3-nucleotide AAA bulge when in complex with PNAzyme I (b) Structure of the dimethyl-dipyridophenazine (dppz) "molecular scissors" moiety which was conjugated to PNA to create Zn^{2+} dimethyl-dppz PNAzymes (c) Previously reported (by Luige *et al*, *Chem. Commun.*, 2021, **57**, 10911-10914 (paper II)) IEX-HPLC chromatogram showing the extent of (site-specific) cleavage of RNA 1 by Zn^{2+} PNAzyme I after 50 min of incubation at 37 °C, pH 7.0. This figure is reproduced from Luige *et al*, *RSC Advances*, 2022, 12, 5398-5406 (paper III).

In the RNA 2-5/PNAzyme II-V complexes (Fig 23), the long recognition arm has been extended by one base pair, compared to the previously studied complexes (RNA 1/PNAzyme I in paper III and Fig 21). The elongation of the recognition arm did not have a significant effect on the RNA cleavage, as the cleavage of RNA 2 by PNAzyme II was shown to be analogous

to the cleavage of RNA 1 by PNAzyme I. However, the cleavage activity decreased somewhat when the bulge-closing base pair was replaced with a GC (Fig 23). Moreover, the weaker AT and UA bulge-closing base pairs in the long recognition arm led to a significant decrease in the cleavage rate, as RNA cleavage half-lives in the range of 11 and 4 h were observed in RNA 4/PNAzyme IV and RNA 5/PNAzyme V complexes, respectively. Cleavage took place in the AA/A site in the bulge, as identified by MS analysis. In the slowest system (RNA 4/PNAzyme IV), substantial cleavage was also noted at the AAA/G site.

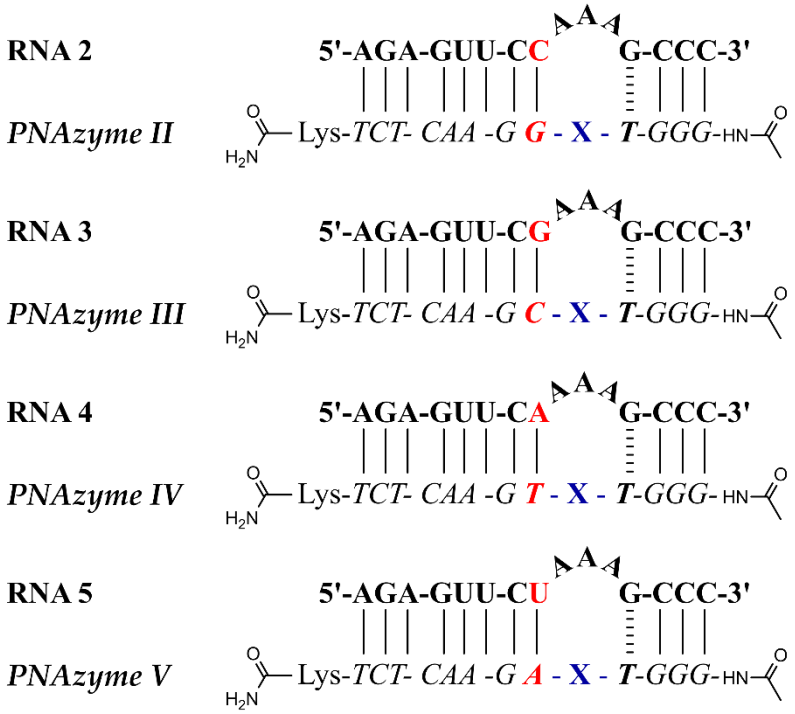

RNA	RNA sequence - N-**bulge** -	PNAzyme	% RNA cleaved		
			0.5 h	1 h	1.5 h
2	-C-**AAA**-	*II*	25	45	59
3	-G-**AAA**-	*III*	16	31	54
4	-A-**AAA**-	*IV*	3	5	13
5	-U-**AAA**-	*V*	6	16	30

Figure 23. Schematic representations of RNA/PNAzyme complexes where the bulge-closing base pair in the long recognition arm varies, followed by the extent of RNA cleavage observed in each complex after incubation of the RNA/PNAzyme complex (4 µM) in the presence of Zn^{2+} (100 µM) at 37 °C, pH 7. The structure of X is shown in Fig 22b. This figure is reproduced from Luige *et al*, *RSC Advances*, 2022, 12, 5398-5406 (paper III).

The key determinant appeared to be the strength of hydrogen bonding in the bulge-closing region in the long recognition arm, but the direction of the base pair was an additional component influencing the activity. Comparing the performance of CG vs GC base pair and UA vs AT pair as the bulge-closing base pair in the long recognition arm suggests that it is beneficial to have the pyrimidine in RNA and purine in the PNA strand in the complexes at hand. As such, it is likely that the stacking interactions with the neighbouring nucleobases play a role in defining the structural arrangement.

In the complexes studied thus far, the bulge-closing base pair in the long recognition arm has been preceded by CG or UA (*i.e.* pyrimidine in RNA, purine in PNA) base pair. As such, the favoured sequences in the region immediately preceding the bulge are pyrimidine-C in RNA and purine-G in PNA, where the C and G form the bulge-closing base pair. Nonetheless, the feasibility of the reverse arrangement should be considered in future work. If the neighbouring base pair were reversed, perhaps GC would become the favoured bulge-closing base pair instead of CG, hence resulting in purine-G sequence in RNA and pyrimidine-C in PNA. Interestingly, in more complicated triplex clamp-forming Cu^{2+}-dependent neocuproine-based PNAzymes, indeed the sequence AG (purine-G) was favoured over AC in RNA and TC (pyrimidine-C) over TG in PNA in the bulge-closing region on the 5' side.[88]

The critical role of the bulge-closing base pair suggests that it has a profound effect on defining the structure of the cleavage site. The RNA 2-5/PNAzyme II-V complexes were analysed by CD spectroscopy to determine whether structural changes occur within the complexes. Indeed, spectral shifts were detected (Fig 24).

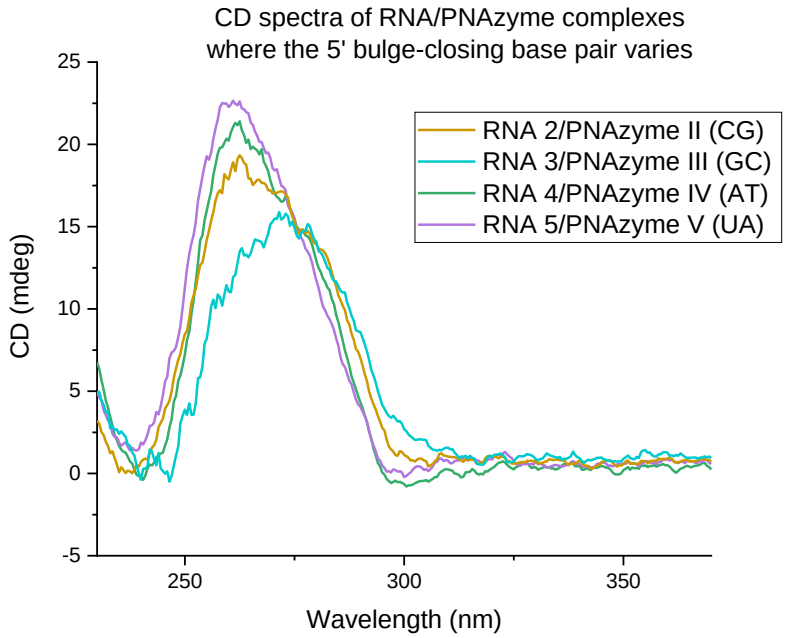

Figure 24. Circular Dichroism (CD) spectra of RNA/PNAzyme complexes where the bulge-closing base pair in the long recognition arm is either CG, GC, AT or UA. This figure is reproduced from Luige *et al*, *RSC Advances*, 2022, 12, 5398-5406 (SI) (paper III).

Improvements in the rate of RNA cleavage by the less efficient PNAzymes (forming UA or AT bulge-closing base pairs) were observed upon varying the bulge sequence. Notably, an RNA target forming an AUA bulge closed with a UA bulge-closing base pair in the long recognition arm was cleaved at a significantly higher rate than the initially studied AAA bulge when closed with the same base pair. The estimated cleavage half-life was in the range of 1.5 h. Moreover, the PNAzyme forming an AT bulge-closing base pair in the long recognition arm showed increased activity for the cleavage of 2-nucleotide bulges with an approximately 1.5 h cleavage half-life observed for the UU bulge. Nonetheless, these developments could not

compete with the previously identified fastest cleavage rates of UUA, AUA and GUA bulges (16 min at pH 7.0) closed with a CG base pair in the long recognition arm.

5.3.2 Sequence variation in the short recognition arm

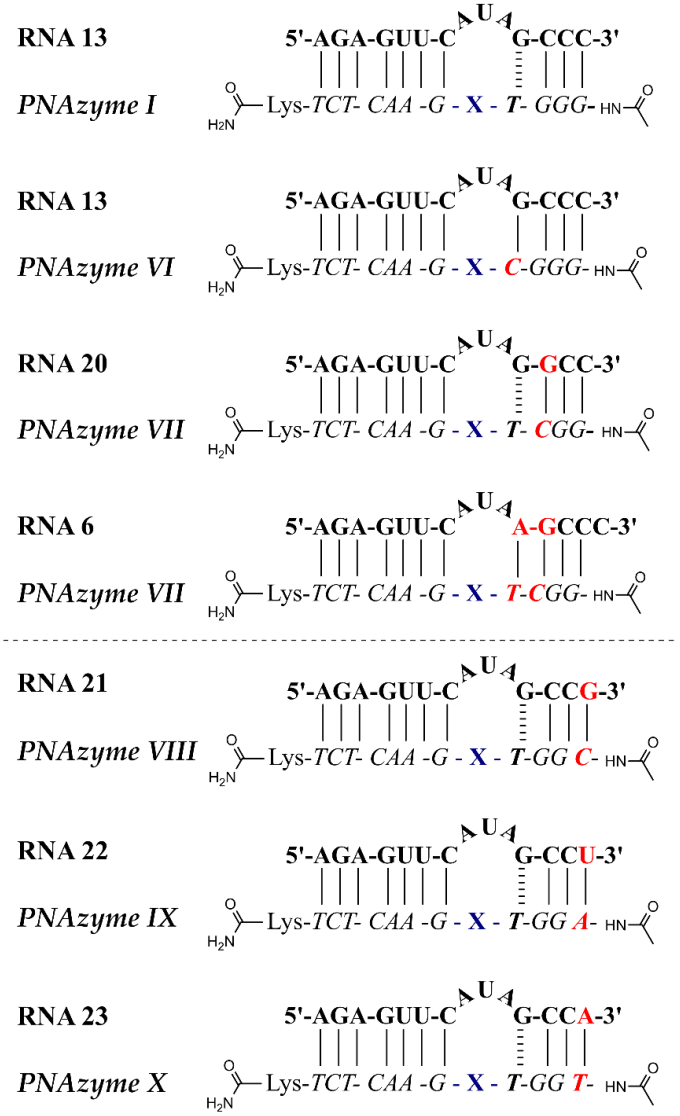

RNA	PNAzyme	% RNA cleaved	
		10 min	20 min
13	*I*	35*	58*
13	*VI*	3	9
20	*VII*	17	39
6	*VII*	8	18
21	*VIII*	36	57
22	*IX*	29	52
23	*X*	25	50

Figure 25. Schematic representation of RNA/PNAzyme complexes containing variations in the short recognition arm sequence, followed by the extent of RNA cleavage observed in each complex after incubation of the RNA/PNAzyme complex (4 µM) in the presence of Zn^{2+} (100 µM) at 37 °C, pH 7. The structure of "X" is shown in Fig 22b. *The extent of cleavage of RNA 13 by PNAzyme I has been previously reported by Luige *et al*, *Chem. Commun.*, 2021, **57**, 10911-10914 (paper II). This figure is reproduced from Luige *et al, RSC Advances*, 2022, 12, 5398-5406 (paper III).

The bulge-closing base pair on the 3' side, in the short recognition arm was then varied (Fig 25). The replacement of the GT wobble base pair (PNAzyme I in paper III) with a GC Watson-Crick base pair (PNAzyme VI in paper III) significantly lowered the RNA cleavage rate, similarly to the previous Cu^{2+}-neocuproine PNAzymes that were based on the same recognition arm sequences.[89]

The change from a weak GT wobble to a strong GC Watson-Crick base pair had a significant effect on the CD spectrum of the complex (Fig 26), suggesting that the structure of the complex was indeed profoundly affected.

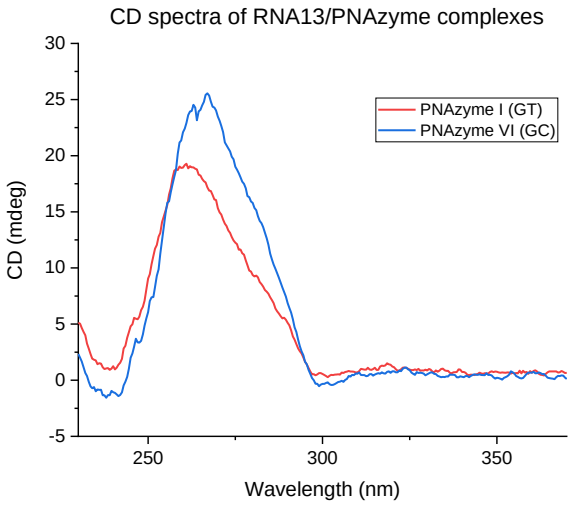

Figure 26. Circular Dichroism (CD) spectra of RNA 13 complexes with PNAzyme I and VI where the bulge-closing base pair in the short recognition arm is a GT wobble or a GC base pair. This figure is reproduced from Luige *et al*, *RSC Advances*, 2022, 12, 5398-5406 (SI) (paper III).

When the GT wobble was succeeded by a GC (RNA 25) instead of a CG base pair, the cleavage rate dropped slightly, suggesting once again that the intra-strand stacking interactions have a role in influencing the bulge. As the RNA sequence GC (purine-pyrimidine) was favoured over GG (purine-purine) in this part of the sequence, it is possible that the GU (purine-pyrimidine) RNA sequence would be tolerated over GA (purine-purine). In future studies, the importance of the strength of hydrogen bonding between the base pair next to the GT wobble should be investigated to determine whether the GT bulge-closing base pair in the short recognition arm could indeed be followed by a UA base pair.

When the same system was further modified to include an AT bulge-closing base pair, a further decrease in the cleavage rate was observed. Clearly, the GT wobble is necessary as the bulge-closing base pair in the short recognition arm, while AT in its place leads to lower activity and GC even more so. In contrast, sequence variation at the terminus of the short recognition arm (RNAs 21-23 in paper III) did not have a significant effect on the RNA cleavage rate.

In conclusion, these results indicate that the PNAzyme activity is highly influenced by the sequence in the bulge closing regions on both sides. As such, the selection of novel RNA targets should be based on identifying sequences containing one of the preferred bulge sequences that is surrounded by the critical bulge-closing sequences, as depicted in Fig 27.

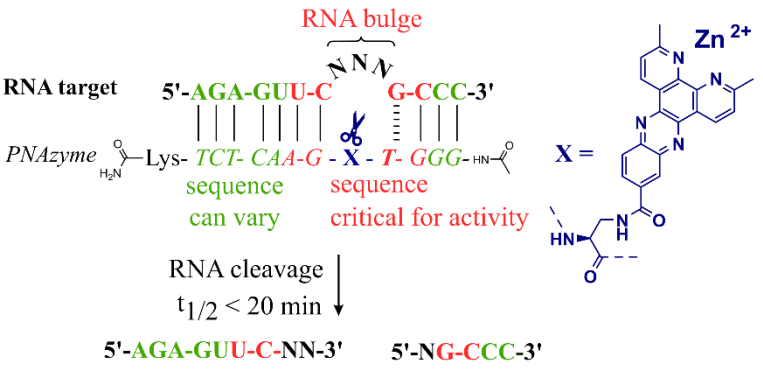

Figure 27. Summary of the influence of sequence variation in the double-stranded recognition arms of RNA/PNAzyme complexes, showing parts of the sequence where variations are tolerated (green) versus not tolerated (red). This figure is reproduced from Luige *et al*, *RSC Advances*, 2022, 12, 5398-5406 (paper III).

5.3.3 Elongation of the complex

Elongation of the short recognition arm of the RNA/ Zn^{2+}-dimethyl-dppz PNAzyme complex by 2 and 4 base pairs was investigated. The complexes studied in paper III had the RNA short recognition arm sequences 5'-GCCC-3', 5'-GCCCUU-3' and 5'-GCCCUUAG-3'. In such complexes, where the recognition arms were fully hybridised, the length of the short recognition arm as shown not to affect the RNA cleavage activity (Fig 28). Moreover, the elongated PNAzyme XII was shown to give turnover with a 33-fold excess of the RNA 25, although the extent of RNA cleavage after 6 h was higher with the shorter complex under the same conditions in paper II, suggesting that dissociation of the complex post-cleavage becomes limiting in the elongated complex.

However, RNA cleavage was slower in complexes where the RNA short recognition arm consisting of the sequence 5'-GCCC-3' was paired with the elongated PNAzymes, leading to a PNAzyme overhang. Interestingly, the presence of a PNAzyme overhang decreased the cleavage rate, which was also previously noted for Cu^{2+}-neocuproine PNAzymes (paper I). On the other hand, the RNA overhang in the RNA 25/ PNAzyme I complex did not affect the rate of RNA cleavage, suggesting that the PNAzyme is able to efficiently promote the cleavage of longer RNA targets.

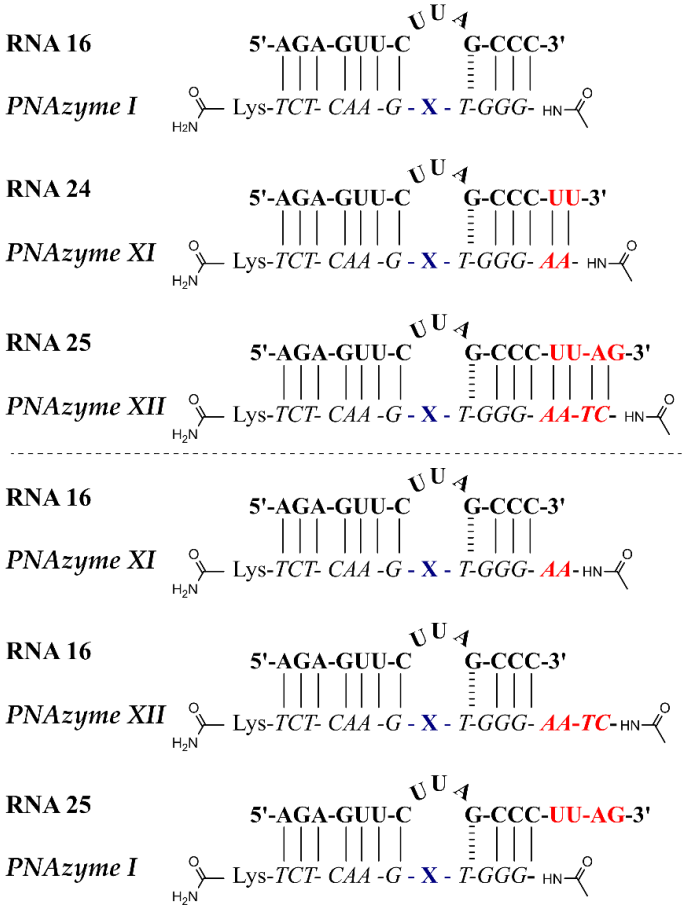

RNA	PNAzyme	% RNA cleaved	
		10 min	20 min
16	*I*	37*	60*
24	*XI*	33	57
25	*XII*	38	59
16	*XI*	29	45
16	*XII*	26	48
25	*I*	34	59

Figure 28. Schematic representations of complexes of elongated RNA/PNAzyme, followed by the extent of RNA cleavage observed in each complex after incubation of the RNA/PNAzyme complex (4 µM) in the presence of Zn^{2+} (100 µM) at 37 °C, pH 7. The structure of "X" is shown in Fig 22b. This figure is reproduced from Luige *et al*, *RSC Advances*, 2022, 12, 5398-5406 (paper III).

5.3.4 Sequence dependence in the cleavage of 4-nucleotide bulges

The 4-nucleotide AAAA bulge-forming RNA target 1 was shown to be cleaved with a ca 3 h half-life in paper II. Moreover, in contrast to the cleavage of 3-nucleotide bulges by the Zn^{2+}-dimethyl-dppz PNAzyme, the cleavage of the AAAA bulge-forming RNA target is not site-specific, but instead takes place at two equally favoured cleavage sites, namely 5'-AA/-AA-3' or 5'-AAA/A-3'.

The cleavage of 4-nucleotide bulges showed significant bulge sequence dependence. RNA targets forming UAAA, AUAA, AAUA, UUAA and UAUA bulges (Fig 29) were cleaved

significantly faster than the initial target (RNA 4). The half-life of RNA cleavage was reduced to approximately 1 h for the UAUA bulge. Moreover, the cleavage of the UAUA bulge was also highly site-selective, taking place predominantly between the third and fourth nucleotide (*i.e.* 5'-UAU/A-3'). In the context of possible future applications for the Zn^{2+}-dimethyl-dppz PNAzymes, the presence of such 4-nucleotide bulge-forming RNA sequences could give rise to potential off-target cleavage.

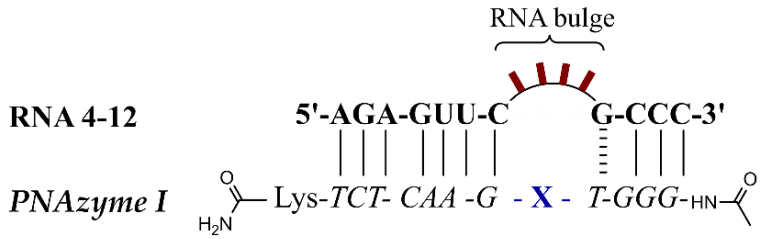

RNA	RNA bulge sequence	% RNA cleaved 1 h	% RNA cleaved 3 h
4	**-AAAA-**	18	51*
5	**-UAAA-**	39	78
6	**-AUAA-**	39	77
7	**-AAUA-**	24	64
8	**-AAAU-**	14	33
9	**-AAUU-**	7	20
10	**-UUAA-**	40	79
11	**-UAUA-**	55	89
12	**-UUUA-**		52

Figure 29. Schematic representations of RNA/PNAzyme complexes where 4-nucleotide RNA bulges are formed, followed by the extent of RNA cleavage observed in each complex after incubation of the RNA/PNAzyme complex (4 µM) in the presence of Zn^{2+} (100 µM) at 37 °C, pH 7. The structure of "X" (the "molecular scissors") is shown in Fig 22b. *The extent of cleavage of RNA 4 by PNAzyme I in 3 h has been previously reported in paper II. This figure is reproduced from Luige *et al*, *RSC Advances*, 2022, 12, 5398-5406 (paper III).

6 CONCLUSIONS

This thesis described studies on PNA-based artificial ribonucleases (PNAzymes), which included further studies on Cu^{2+}-dependent PNA-neocuproine conjugates and the development of Zn^{2+}-dependent PNA-dimethyl-dppz conjugates as efficient site-specific artificial RNA-cutting enzymes. These PNAzymes could be of utility as research tools in molecular biology or as therapeutics to target endogenous disease-related RNA for medical intervention.

Paper I:

Cu^{2+}-dependent PNA-neocuproine conjugates were shown to be able to cleave 3-nucleotide RNA bulges, albeit at a significantly slower rate than the previously described 4-nucleotide bulge-forming RNA targets. The activity was shown to be significantly influenced by the bulge sequence in a similar manner to the previously described 4-nucleotide bulges.

Further insights into the cleavage mechanism of the fastest cleaved AUAA bulge were derived, as the Cu^{2+}-neocuproine PNAzyme-mediated RNA cleavage was shown to be critically dependent on the presence of the exocyclic amino group and the 2'-hydroxyl group in the adenosine (A*) nucleotide in the 5'-AUA*A-3' bulge. Moreover, "pin-point" phosphodiester activation by interactions with a polyaromatic molecule was shown not to be relevant in the case of these PNAzymes, as a PNA-phenanthrene conjugate was not able to promote RNA cleavage despite the presence of added Cu^{2+} ions.

Elongation of the RNA/PNAzyme complex by 2 base pairs in the long recognition arm was shown to leave the RNA cleavage rate unaffected, while allowing to maintain the cleavage efficiency of a significantly longer RNA target sequence that contained partial competing recognition arm sequences, thus resembling a more likely natural target. A short PNAzyme overhang was shown to decrease the cleavage activity, further demonstrating the highly sequence-specific nature of PNAzymes.

Paper II:

The development of novel biocompatible Zn^{2+}-dependent artificial ribonucleases containing dimethyl-dipyridophenazine as "molecular scissors" in the PNAzyme structure was described. The dependence of their activity on the RNA bulge sequence, pH and Zn^{2+} ion concentration was studied in detail. The initial target, a leukaemia-related bcr/abl mRNA model that forms a 4-nucleotide AAAA bulge was cleaved with a 3 h half-life at two cleavage sites, while a shorter 3-nucleotide AAA bulge was cleaved with a 1 h half-life at a single site. Altering the 3-nucleotide bulge sequence revealed further improvements, as the fastest cleavage (16 min half-lives at pH 7.0) was observed for UUA, AUA and GUA bulge sequences, while other 3-nucleotide bulges were cleaved slowly or were shown to be essentially uncleavable.

The Zn^{2+}-dimethyl-dppz PNAzyme-promoted RNA cleavage had a bell-shaped pH-rate profile. RNA cleavage was shown to occur at a single site with down to 10-minute half-lives at pH 7.4. The Zn^{2+}-dimethyl-dppz PNAzymes were thus shown to outperform all previously

published artificial ribonucleases. Moreover, they were shown to be capable of cleaving clinically relevant RNA sequences, namely a *Plasmodium falciparum* (malaria parasite) mRNA model and a SARS-CoV-2 genomic RNA model.

Paper III:

The influence of sequence variation on the RNA cleavage activity of the Zn^{2+}-dependent dimethyl-dipyridophenazine PNAzymes was studied in detail. The RNA target sequence was shown to be highly significant, both in the single-stranded bulge region and in the hybridised bulge-closing regions. The replacement of the CG bulge-closing base pair in the long recognition arm with a GC pair led to a slightly reduced cleavage rate, while a UA or AT base pair in this position resulted in a remarkable decrease in activity. In the short recognition arm, GT wobble was shown to be required as the bulge-closing base pair, as an AT or GC base pair led to a significant decrease in the activity. In addition to the bulge-closing base pairs, the neighbouring base pairs in the double stranded regions are suggested to be influential. The terminal base pairs in the short recognition arm were shown not to significantly affect the cleavage activity. Moreover, elongation of the short recognition arm was shown to be tolerated, but potentially prohibitive for catalytic turnover.

In addition, the bulge sequence dependence of 4-nucleotide bulge-forming RNA targets was investigated. Cleavage half-lives down to 1 h were demonstrated for select bulge sequences where the cleavage was nearly site-specific. As such, potential off-target cleavage of 4-nucleotide bulge-forming RNAs should be considered.

In conclusion, RNA target sequences containing the sequence 5'-Py-C-bulge-GC-3' (where the bulge is AUA, UUA or GUA) are suggested to be efficiently cleaved by PNAzymes, while future studies could investigate the feasibility of the RNA sequences 5'-Pu-G-bulge-GC-3' and 5'-Py-C-bulge-GU-3' as targets for PNAzyme-mediated RNA cleavage. The unprecedented efficiency and specificity of Zn^{2+} dimethyl-dppz PNAzymes will hopefully inspire future investigations to assess their efficacy in biological settings.

7 POINTS OF PERSPECTIVE

Oligonucleotide-based artificial ribonucleases hold enormous potential as tools for nucleic acid manipulation for biological intervention. The research presented in this thesis deepened the understanding of Cu^{2+}-neocuproine PNAzymes and described novel Zn^{2+}-dependent dimethyl-dipyridophenazine PNAzymes that act as artificial RNA-cutting enzymes and exhibit unprecedented efficiency and specificity. The RNA cleavage rates displayed by Zn^{2+}-dimethyl-dppz PNAzymes outperform all previously published artificial ribonucleases and give turnover of the substrate. These novel artificial ribonucleases rely on the presence of Zn^{2+} ions, which makes them more biocompatible than the previous Cu^{2+} PNAzymes. The influence of sequence variation has been investigated and the possibility to produce efficient tailor-made PNAzymes to degrade clinically relevant RNA models has been demonstrated.

The next step for Zn^{2+}-dependent dimethyl-dppz PNAzymes is testing their activity on significantly longer targets and in biologically relevant environments. Diseases associated with elevated Zn^{2+} concentrations (*e.g.* malaria and Alzheimer's disease) are particularly interesting for future developments. Alternatively, the development of Zn^{2+}-nanoparticle-based PNAzyme delivery systems could enable the PNAzymes to be equipped with a Zn^{2+} supply. Additional strategies for PNAzyme delivery and targeting could be developed. Conjugation to peptides designed to enhance cell penetration and endosomal escape could be investigated.

In addition, both Cu^{2+}-neocuproine and Zn^{2+}-dimethyl-dppz PNAzymes are highly efficient site-specific RNA restriction enzymes that could be developed further for applications in molecular biology research.

8 ACKNOWLEDGEMENTS

I would like to thank everyone who was a part of my PhD journey in the last 4 years – my colleagues and collaborators, my friends and family – thank you! Aitäh!

I would like to thank my main supervisor Prof. **Roger Strömberg** for the opportunity to pursue my PhD in his research group and to apply myself towards the development of PNA-based artificial ribonucleases.

I would like to thank my co-supervisor **Merita Murtola** for teaching me experimental skills for the synthesis, purification and analysis of PNAzymes and for her guidance in navigating challenges, both scientific and non-scientific!

I would like to thank my co-supervisor **Dmytro Honcharenko**, as well as the members of our laboratory – **Malgorzata Honcharenko, Partha Pratim Bose, Dmitri Ossipov and Håkan Ottosson** – for offering advice and guidance throughout this journey! Thank you Partha for your contribution to my second and third paper!

I would like to thank **Kristina Karalė, Martin Bollmark** and **Ulf Tedebark** for being bonus members of our research group and for their contribution to my third paper! Thank you Kristina for being on this journey with me – we have shared so many experiences in the last 4.5 years, from lab work to conferences to dinner parties to taking care of Dash and Millie. Thank you for all your help and for making this time so special!

I would like to thank **Rouven Stulz, Anders Dahlén, Shalini Andersson** and their colleagues at AstraZeneca for welcoming me to your lab for my secondment! Thank you Rouven, Shalini and the Separation Science Laboratory at AstraZeneca for your contribution to my second and third paper!

I would like to thank my co-author **Alice Ghidini** for her contribution to my first paper and for welcoming me to her lab and introducing me to the world of oligonucleotide biophysics during my internship at AstraZeneca!

I would like to thank my co-authors **Peter Steunenberg** and **Omar Brun** for their contribution to my second paper! Your work was so fundamentally important for the development of Zn^{2+} PNAzymes and I am so grateful for it!

I would like to thank all the members of the Marie Curie Innovative Training Network Molecular Tools for Nucleic Acid Manipulation for Biological Intervention (MMBio) that my PhD was a part of! Thank you all for working with me – thank you for the network meetings and for the collaborations and interactions we had during the different secondments. Thank you **Kristina, Rouven** and **Tea** – our MMBio Sweden team! Thank you to the rest of my fellow Early Stage Researchers – **Madhuri, Alisa, Lise, Remkes, Susanna, Konstantinos, Enrico, Valerio, Søren, Lucia** and **Joanna** for being a part of it!

I would like to thank my mentor **Alessandra Villa** for her support and advice throughout my PhD!

Thank you **Tina** for being such a good friend, you made Neo a much better place :) Thanks for "meeting in the middle" for the fika breaks and chats, and for helping me with the nanodrop and CD. Best of luck for the new chapter in your life 💔

Thank you **Eva-Lotta** for helping to advance my understanding of molecular biology and for being a supportive friend throughout my PhD!

Thank you to my sister **Johanna** for your help and support! With molecular biology and beyond. Thank you for the wonderful art on the front cover of my thesis!

Thank you **Padryk** for everything!

9 REFERENCES

1 J. Drews, *Science*, 2000, **287**, 1960–1964.

2 D. E. Scott, A. R. Bayly, C. Abell and J. Skidmore, *Nat. Rev. Drug Discov.*, 2016, **15**, 533–550.

3 C. I. E. Smith and R. Zain, *Annu. Rev. Pharmacol. Toxicol.*, 2019, **59**, 605–630.

4 D. C. Fry, *Biopolymers*, 2006, **84**, 535–552.

5 L. N. Makley and J. E. Gestwicki, *Chem Biol Drug Des*, 2013, **81**, 22–32.

6 E. Uhlmann and A. Peyman, *Chem. Rev.*, 1990, **90**, 543–584.

7 F. Crick, *Nature*, 1970, **227**, 561–563.

8 M. Cobb, *PLoS Biol.*, 2017, **15**, 1–8.

9 S. Crooke, *Antisense Res. Dev.*, 1993, **3**, 1–2.

10 J. Scharner and I. Aznarez, *Mol. Ther.*, 2021, **29**, 540–554.

11 K. Xue and R. E. MacLaren, *Expert Opin. Investig. Drugs*, 2020, **29**, 1163–1170.

12 J. Rüger, S. Ioannou, D. Castanotto and C. A. Stein, *Trends Pharmacol. Sci.*, 2020, **41**, 27–41.

13 C. A. Stein and D. Castanotto, *Mol. Ther.*, 2017, **25**, 1069–1075.

14 A. Khvorova and J. K. Watts, *Nat. Biotechnol.*, 2017, **35**, 238–248.

15 X. Shen and D. R. Corey, *Nucleic Acids Res.*, 2018, **46**, 1584–1600.

16 R. L. Juliano, X. Ming and O. Nakagawa, *Acc. Chem. Res.*, 2012, **45**, 1067–1076.

17 T. C. Roberts, R. Langer and M. J. A. Wood, *Nat. Rev. Drug Discov.*, 2020, **19**, 673–694.

18 A. J. Debacker, J. Voutila, M. Catley, D. Blakey and N. Habib, *Mol. Ther.*, 2020, **28**, 1759–1771.

19 K. Klabenkova, A. Fokina and D. Stetsenko, *Molecules*, 2021, **26**, 5420.

20 K. Craig, M. Abrams and M. Amiji, *Expert Opin. Drug Deliv.*, 2018, **15**, 629–640.

21 J. Micklefield, *Curr. Med. Chem.*, 2001, **8**, 1157–1179.

22 I. Lebedeva and C. Stein, *Annu. Rev. Pharmacol. Toxicol.*, 2001, **41**, 403–419.

23 K. Sridharan and N. J. Gogtay, *Br. J. Clin. Pharmacol.*, 2016, **82**, 659–672.

24 P. E. Nielsen and M. Egholm, *Curr. Issues Mol. Biol.*, 1999, **1**, 89–104.

25 R. L. Juliano, *Nucleic Acids Res.*, 2016, **44**, 6518–6548.

26 P. E. Nielsen, M. Egholm and O. Buchardt, *Bioconjug. Chem.*, 1994, **5**, 3–7.

27 P. E. Nielsen and G. Haaima, *Chem. Soc. Rev.*, 1997, **26**, 73.

28 M. Petersen and J. Wengel, *Trends Biotechnol.*, 2003, **21**, 74–81.

29 A. Laina, A. Gatsiou, G. Georgiopoulos, K. Stamatelopoulos and K. Stellos, *Front. Physiol.*, 2018, **9**, 953.

30 M. Nowotny and W. Yang, *EMBO J.*, 2006, **25**, 1924–1933.

31 H. Nakamura, Y. Oda, S. Iwai, H. Inoue, E. Ohtsuka, S. Kanaya, S. Kimura, C. Katsuda, K. Katayanagi, K. Morikawa, H. Miyashiro and M. Ikehara, *Proc. Natl. Acad. Sci. U. S. A.*, 1991, **88**, 11535–11539.

32 M. Nowotny, S. A. Gaidamakov, R. J. Crouch and W. Yang, *Cell*, 2005, **121**, 1005–1016.

33 K. E. Lundin, O. Gissberg and C. I. E. Smith, *Hum. Gene Ther.*, 2015, **26**, 475–485.

34 M. A. Havens and M. L. Hastings, *Nucleic Acids Res.*, 2016, **44**, 6549–6563.

35 S. Abes, J. J. Turner, G. D. Ivanova, D. Owen, D. Williams, A. Arzumanov, P. Clair, M. J. Gait and B. Lebleu, *Nucleic Acids Res.*, 2007, **35**, 4495–4502.

36 S. A. El Andaloussi, S. M. Hammond, I. Mager and M. J.A. Wood, *Curr. Gene Ther.*, 2012, **12**, 161–178.

37 T. Soudah, M. Mogilevsky, R. Karni and E. Yavin, *Bioconjug. Chem.*, 2017, **28**, 3036–3042.

38 A. Wittrup and J. Lieberman, *Nat. Rev. Genet.*, 2015, **16**, 543–552.

39 P. D. Zamore, *Cell*, 2006, **127**, 1083–1086.

40 A. Reynolds, D. Leake, Q. Boese, S. Scaringe, W. S. Marshall and A. Khvorova, *Nat. Biotechnol.*, 2004, **22**, 326–330.

41 J. Sheu-Gruttadauria and I. J. MacRae, *J. Mol. Biol.*, 2017, **429**, 2619–2639.

42 D. M. Kenski, G. Butora, A. T. Willingham, A. J. Cooper, W. Fu, N. Qi, F. Soriano, I. W. Davies and W. M. Flanagan, *Mol. Ther. - Nucleic Acids*, 2012, **1**, e5.

43 K. M. Bishop, *Neuropharmacology*, 2017, **120**, 56–62.

44 A. D. Keefe, S. Pai and A. Ellington, *Nat. Rev. Drug Discov.*, 2010, **9**, 537–550.

45 M. L. Stephenson and P. C. Zamecnik, *Proc. Natl. Acad. Sci. U. S. A.*, 1978, **75**, 285–288.

46 P. C. Zamecnik and M. L. Stephenson, *Proc. Natl. Acad. Sci. U. S. A.*, 1978, **75**, 280–284.

47 V. K. Sharma and J. K. Watts, *Future Med. Chem.*, 2015, **7**, 2221–2242.

48 J. P. Bost, H. Barriga, M. N. Holme, A. Gallud, M. Maugeri, D. Gupta, T. Lehto, H. Valadi, E. K. Esbjörner, M. M. Stevens and S. El-Andaloussi, *ACS Nano*, 2021, **15**, 13993–14021.

49 A. Aartsma-Rus and D. R. Corey, *Nucleic Acid Ther.*, 2020, **00**, 1–4.

50 Y.-A. Heo, *Drugs*, 2020, **80**, 329–333.

51 S. Dhillon, *Drugs*, 2020, **80**, 1027–1031.

52 R. R. Roshmi and T. Yokota, *Clin. Pharmacol. Adv. Appl.*, 2021, **13**, 235–242.

53 M. Shirley, *Drugs*, 2021, **81**, 875–879.

54 J. Kim, C. Hu, C. M. El Achkar, L. E. Black, J. Douville, A. Larson, M. K. Pendergast, S. F. Goldkind, E. A. Lee, A. Kuniholm, A. Soucy, J. Vaze, N. R. Belur, K. Fredriksen, I. Stojkovska, A. Tsytsykova, M. Armant, R. L. DiDonato, J. Choi, L. Cornelissen, L. M. Pereira, E. F. Augustine, C. A. Genetti, K. Dies, B. Barton, L. Williams, B. D. Goodlett, B. L. Riley, A. Pasternak, E. R. Berry, K. A. Pflock, S. Chu, C. Reed, K. Tyndall, P. B. Agrawal, A. H. Beggs, P. E. Grant, D. K. Urion, R. O. Snyder, S. E. Waisbren, A. Poduri, P. J. Park, A. Patterson, A. Biffi, J. R. Mazzulli, O. Bodamer, C. B. Berde and T. W. Yu, *N. Engl. J. Med.*, 2019, **381**, 1644–1652.

55 S. J. Keam, *Drugs*, 2018, **78**, 1371–1376.

56 S. M. Hoy, *Drugs*, 2018, **78**, 1625–1631.

57 J. L. Witztum, D. Gaudet, S. D. Freedman, V. J. Alexander, A. Digenio, K. R. Williams, Q. Yang, S. G. Hughes, R. S. Geary, M. Arca, E. S. G. Stroes, J. Bergeron, H. Soran, F. Civeira, L. Hemphill, S. Tsimikas, D. J. Blom, L. O'Dea and E. Bruckert, *N. Engl. J. Med.*, 2019, **381**, 531–542.

58 S. Agarwal, A. R. Simon, V. Goel, B. A. Habtemariam, V. A. Clausen, J. B. Kim and G. J. Robbie, *Clin. Pharmacol. Ther.*, 2020, **0**, 1–10.

59 C. A. German and M. D. Shapiro, *BioDrugs*, 2020, **34**, 1–9.

60 K. Dyrbuś, M. Gąsior, P. Penson, K. K. Ray and M. Banach, *J. Clin. Lipidol.*, 2020, **14**, 16–27.

61 B. Tomlinson, E. Chow, P. Chan and C. W. K. Lam, *Expert Opin. Drug Metab. Toxicol.*, 2022, **00**, 1–9.

62 Y. N. Lamb, *Drugs*, 2021, **81**, 389–395.

63 L. J. Scott and S. J. Keam, *Drugs*, 2021, **81**, 277–282.

64 M. M. Attwood, M. Rask-Andersen and H. B. Schiöth, *Trends Pharmacol. Sci.*, 2018, **39**, 525–535.

65 R. L. Juliano, *Nucleic Acid Ther.*, 2018, **28**, 166–177.

66 P. P. Seth, M. Tanowitz and C. Frank Bennett, *J. Clin. Invest.*, 2019, **129**, 915–925.

67 L. Gales, *Pharmaceuticals*, 2019, **12**, 10–15.

68 T. Gökirmak, M. Nikan, S. Wiechmann, T. P. Prakash, M. Tanowitz and P. P. Seth, *Trends Pharmacol. Sci.*, 2021, **42**, 588–604.

69 W. Yang, *Nucleases: Diversity of structure, function and mechanism*, 2011, vol. 44.

70 L. Ma and J. Liu, *iScience*, 2020, **23**, 1–17.

71 D. Hüsken, G. Goodall, M. J. J. Blommers, W. Jahnke, J. Hall, R. Häner and H. E. Moser, *Biochemistry*, 1996, **35**, 16591–16600.

72 M. J. Fedor and J. R. Williamson, *Nat. Rev. Mol. Cell Biol.*, 2005, **6**, 399–412.

73 S. Mikkola, T. Lönnberg and H. Lönnberg, *Beilstein J. Org. Chem.*, 2018, **14**, 803–837.

74 F. Guo, Z. Yue, M. Trajkovski, X. Zhou, D. Cao, Q. Li, B. Wang, X. Wen, J. Plavec, Q. Peng, Z. Xi and C. Zhou, *J. Am. Chem. Soc.*, 2018, **140**, 11893–11897.

75 C. M. Cuchillo, M. V. Nogués and R. T. Raines, *Biochemistry*, 2011, **50**, 7835–7841.

76 M. Hyjek, M. Figiel and M. Nowotny, *DNA Repair*, 2019, **84**, 102672.

77 A. Ghidini, M. Murtola and R. Strömberg, in *DNA in Supramolecular Chemistry and Nanotechnology*, John Wiley & Sons, Ltd, Chichester, UK, 1st Ed., 2017, pp. 158–171.

78 A. Kuzuya and M. Komiyama, *Curr. Org. Chem.*, 2007, **11**, 1450–1459.

79 Y. Wang, A. Vorperian, M. Shehabat and J. C. Chaput, *ChemBioChem*, 2020, **21**, 1001–1006.

80 Y. Wang, A. K. Ngor, A. Nikoomanzar and J. C. Chaput, *Nat. Commun.*, 2018, **9**, 1–10.

81 T. Niittymäki and H. Lönnberg, *Org. Biomol. Chem.*, 2006, **4**, 15–25.

82 D. Magda, M. Wright, S. Crofts, A. Lin and J. L. Sessler, *J. Am. Chem. Soc.*, 1997, **119**, 6947–6948.

83 R. B. Van Order and H. G. Lindwall, *Chem. Rev.*, 1942, 30, 69–96.

84 J. Hall, D. Hüsken and R. Häner, *Nucleic Acids Res.*, 1996, **24**, 3522–3526.

85 L. Canaple, D. Hüsken, J. Hall and R. Häner, *Bioconjug. Chem.*, 2002, **13**, 945–951.

86 S. Sakamoto, T. Tamura, T. Furukawa, Y. Komatsu, E. Ohtsuka, M. Kitamura and H. Inoue, *Nucleic Acids Res.*, 2003, **31**, 1416–1425.

87 M. Murtola, A. Ghidini, P. Virta and R. Strömberg, *Molecules*, 2017, **22**, 1856.

88 A. Ghidini, M. Murtola and R. Strömberg, *Org. Biomol. Chem.*, 2016, **14**, 2768–2773.

89 M. Murtola, M. Wenska and R. Strömberg, *J. Am. Chem. Soc.*, 2010, **132**, 8984–8990.

90 A. Whitney, G. Gavory and S. Balasubramanian, *Chem. Commun.*, 2003, 36–37.

91 Y. Staroseletz, S. Gaponova, O. Patutina, E. Bichenkova, B. Amirloo, T. Heyman, D. Chiglintseva and M. Zenkova, *Molecules*, 2021, **26**, 1732.

92 F. Zellmann, L. Thomas, U. Scheffer, R. K. Hartmann and M. W. Göbel, *Molecules*, 2019, **24**, 807.

93 F. Danneberg, A. Ghidini, P. Dogandzhiyski, E. Kalden, R. Strömberg and M. W. Göbel, *Beilstein J. Org. Chem.*, 2015, **11**, 493–498.

94 C. Gnaccarini, S. Peter, U. Scheffer, S. Vonhoff, S. Klussmann and M. W. Göbel, *J. Am. Chem. Soc.*, 2006, **128**, 8063–8067.

95 U. Scheffer, A. Strick, V. Ludwig, S. Peter, E. Kalden and M. W. Göbel, *J. Am. Chem. Soc.*, 2005, **127**, 2211–2217.

96 P. Dogandzhiyski, A. Ghidini, F. Danneberg, R. Strömberg and M. W. Göbel,

Bioconjug. Chem., 2015, **26**, 2514–2519.

97 F. Zellmann and M. W. Göbel, *Molecules*, 2020, **25**, 1842.

98 O. A. Patutina, S. K. Miroshnichenko, N. L. Mironova, A. V. Sen'kova, E. V. Bichenkova, D. J. Clarke, V. V. Vlassov and M. A. Zenkova, *Front. Pharmacol.*, 2019, **10**, 879.

99 Y. Staroseletz, B. Amirloo, A. Williams, A. Lomzov, K. K. Burusco, D. J. Clarke, T. Brown, M. A. Zenkova and E. V. Bichenkova, *Nucleic Acids Res.*, 2020, **48**, 10662–10679.

100 O. Patutina, D. Chiglintseva, E. Bichenkova, S. Gaponova, N. Mironova, V. Vlassov and M. Zenkova, *Molecules*, 2020, **25**, 2459.

101 A. Williams, Y. Staroseletz, M. A. Zenkova, L. Jeannin, H. Aojula and E. V. Bichenkova, *Bioconjug. Chem.*, 2015, **26**, 1129–1143.

102 Y. Staroseletz, A. Williams, K. K. Burusco, I. Alibay, V. V. Vlassov, M. A. Zenkova and E. V. Bichenkova, *Biomaterials*, 2017, **112**, 44–61.

103 B. Amirloo, Y. Staroseletz, S. Yousaf, D. J. Clarke, T. Brown, H. Aojula, M. A. Zenkova and E. V Bichenkova, *Nucleic Acids Res.*, 2022, **50**, 651–673.

104 M. Murtola and R. Strömberg, *Arkivoc*, 2009, 84–94.

105 M. Murtola and R. Strömberg, *Org. Biomol. Chem.*, 2008, **6**, 3837–3842.

106 H. Åström and R. Strömberg, *Org. Biomol. Chem.*, 2004, **2**, 1901–1907.

107 H. Åström, N. H. Williams and R. Strömberg, *Org. Biomol. Chem*, 2003, **1**, 1461–1465.

108 D. W. Domaille, E. L. Que and C. J. Chang, *Nat. Chem. Biol.*, 2008, **4**, 168–175.

109 T. Hara, T. aki Takeda, T. Takagishi, K. Fukue, T. Kambe and T. Fukada, *J. Physiol. Sci.*, 2017, **67**, 283–301.

110 Z. N. Baker, P. A. Cobine and S. C. Leary, *Metallomics*, 2017, **9**, 1501–1512.

111 J. D. Puglisi and I. Tinoco, *Methods Enzymol.*, 1989, **180**, 304–325.

112 M. Murtola, A. Ghidini and R. Strömberg, *Sch. Acad. J. Pharm.*, 2017, **6**, 108–112.

113 J. Sandbrink, M. Murtola and R. Strömberg, *Nucleosides, Nucleotides and Nucleic Acids*, 2007, **26**, 1485–1489.

114 H. Åström and R. Strömberg, *Nucleosides, Nucleotides and Nucleic Acids*, 2001, **20**, 1385–1388.

115 A. M. S. Garas and R. S. Vagg, *J. Heterocycl. Chem.*, 2000, **37**, 151–158.

116 J. M. Butler, P. Jiang-Baucom, M. Huang, P. Belgrader and J. Girard, *Anal. Chem.*, 1996, **68**, 3283–3287.

117 M. D. Struthers, R. P. Cheng and B. Imperiali, *Science*, 1996, **271**, 342–345.

118 E. B. Van der Tol, H. J. Van Ramesdonk, J. W. Verhoeven, F. J. Steemers, E. G. Kerver, W. Verboom and D. N. Reinhoudt, *Chem. - A Eur. J.*, 1998, **4**, 2315–2323.

119 T. Hermann and D. J. Patel, *Structure*, 2000, **8**, 47–54.

120 B. N. Macchion, R. Strömberg and L. Nilsson, *J. Biomol. Struct. Dyn.*, 2008, **26**, 163–173.

121 A. Kuzuya, R. Mizoguchi, F. Morisawa, K. Machida and M. Komiyama, *J. Am. Chem. Soc.*, 2002, **124**, 6887–6894.

122 A. Kuzuya, K. Machida, R. Mizoguchi and M. Komiyama, *Bioconjug. Chem.*, 2002, **13**, 365–369.

123 D. Beyersmann, *Materwiss. Werksttech.*, 2002, **33**, 764–769.

124 A. Mukherjee and W. D. Sasikala, in *Advances in Protein Chemistry and Structural Biology*, Academic Press, Elsevier Inc., 2013, vol. 92, pp. 1–62.

125 G. Li, L. Sun, L. Ji and H. Chao, *Dalt. Trans.*, 2016, **45**, 13261–13276.

126 A. E. Friedman, J. K. Barton, J. C. Chambron, J. P. Sauvage, N. J. Turro and J. K. Barton, *J. Am. Chem. Soc.*, 1990, **112**, 4960–4962.

127 A. J. McConnell, H. Song and J. K. Barton, *Inorg. Chem.*, 2013, **52**, 10131–10136.

128 S. T. Li, Z. Y. Ma, X. Liu, J. L. Tian and S. P. Yan, *Appl. Organomet. Chem.*, 2017, **31**, 1–14.

129 J. R. Morrow and O. Iranzo, *Curr. Opin. Chem. Biol.*, 2004, **8**, 192–200.

130 W. Maret, *Int. J. Mol. Sci.*, 2017, **18**, 2285.

131 I. Sekler, S. L. Sensi, M. Hershfinkel and W. F. Silverman, *Mol. Med.*, 2007, **13**, 337–343.

132 R. B. Franklin, J. Ma, J. Zou, Z. Guan, B. I. Kukoyi, P. Feng and L. C. Costello, *J. Inorg. Biochem.*, 2003, **96**, 435–442.

133 N. K. Wills, V. M. Sadagopa Ramanujam, N. Kalariya, J. R. Lewis and F. J. G. M. van Kuijk, *Exp. Eye Res.*, 2008, **87**, 80–88.

134 R. G. Marvin, J. L. Wolford, M. J. Kidd, S. Murphy, J. Ward, E. L. Que, M. L. Mayer, J. E. Penner-Hahn, K. Haldar and T. V. O'Halloran, *Chem. Biol.*, 2012, **19**, 731–741.

135 A. Abelein, A. Gräslund and J. Danielsson, *Proc. Natl. Acad. Sci. U. S. A.*, 2015, **112**, 5407–5412.

136 T. J. A. Craddock, J. A. Tuszynski, D. Chopra, N. Casey, L. E. Goldstein, S. R. Hameroff and R. E. Tanzi, *PLoS One*, 2012, **7**, e33552.

137 World malaria report 2020: 20 years of global progress and challenges. Geneva: World Health Organization; 2020. Licence: CC BY-NC-SA 3.0 IGO.

138 B. Blasco, Di. Leroy and D. A. Fidock, *Nat. Med.*, 2017, **23**, 917–928.

139 R. G. Marvin, J. L. Wolford, M. J. Kidd, S. Murphy, J. Ward, E. L. Que, M. L. Mayer, J. E. Penner-Hahn, K. Haldar and T. V. O'Halloran, *Chem. Biol.*, 2012, **19**, 731–741.

140 M. Zhang, C. Wang, T. D. Otto, J. Oberstaller, X. Liao, S. R. Adapa, K. Udenze, I. F. Bronner, D. Casandra, M. Mayho, J. Brown, S. Li, J. Swanson, J. C. Rayner, R. H. Y.

Jiang and J. H. Adams, *Science*, , DOI:10.1126/science.aap7847.

141 W. Noonpakdee, J. Pothikasikorn, W. Nimitsantiwong and P. Wilairat, *Biochem. Biophys. Res. Commun.*, 2003, **302**, 659–664.

142 F. Föger, W. Noonpakdee, B. Loretz, S. Joojuntr, W. Salvenmoser, M. Thaler and A. Bernkop-Schnürch, *Int. J. Pharm.*, 2006, **319**, 139–146.

143 K. Günther, M. Tümmler, H. H. Arnold, R. Ridley, M. Goman, J. G. Scaife and K. Lingelbach, *Mol. Biochem. Parasitol.*, 1991, **46**, 149–157.

144 P. Mesén-Ramírez, B. Bergmann, T. T. Tran, M. Garten, J. Stäcker, I. Naranjo-Prado, K. Höhn, J. Zimmerberg and T. Spielmann, *PLoS Biol.*, 2019, **17**, 1–33.

145 K. B. Spurgers, C. M. Sharkey, K. L. Warfield and S. Bavari, *Antiviral Res.*, 2008, **78**, 26–36.

146 D. Shin, R. Mukherjee, D. Grewe, D. Bojkova, K. Baek, A. Bhattacharya, L. Schulz, M. Widera, A. R. Mehdipour, G. Tascher, P. P. Geurink, A. Wilhelm, G. J. van der Heden van Noort, H. Ovaa, S. Müller, K. P. Knobeloch, K. Rajalingam, B. A. Schulman, J. Cinatl, G. Hummer, S. Ciesek and I. Dikic, *Nature*, 2020, **587**, 657–662.